Published in Sedimentary Geology 173: 187–232, 2005

The stratigraphic architecture and evolution of the Burdigalian carbonate—siliciclastic sedimentary systems of the Mut Basin, Turkey

P. Bassant[a,*], F.S.P. Van Buchem[a], A. Strasser[b], N. Görür[c]

[a]*Institut Français du Pétrole, Rueil-Malmaison, France*
[b]*University of Fribourg, Switzerland*
[c]*Istanbul Technical University, Istanbul, Turkey*

Received 17 February 2003; received in revised form 18 November 2003; accepted 21 January 2004

Abstract

This study describes the coeval development of the depositional environments in three areas across the Mut Basin (Southern Turkey) throughout the Late Burdigalian (early Miocene). Antecedent topography and rapid high-amplitude sea-level change are the main controlling factors on stratigraphic architecture and sediment type. Stratigraphic evidence is observed for two high-amplitude (100–150 m) sea-level cycles in the Late Burdigalian to Langhian. These cycles are interpreted to be eustatic in nature and driven by the long-term 400-Ka orbital eccentricity-cycle-changing ice volumes in the nascent Antarctic icecap. We propose that the Mut Basin is an exemplary case study area for guiding lithostratigraphic predictions in early Miocene shallow-marine carbonate and mixed environments elsewhere in the world.

The Late Burdigalian in the Mut Basin was a time of relative tectonic quiescence, during which a complex relict basin topography was flooded by a rapid marine transgression. This area was chosen for study because it presents extraordinary large-scale 3D outcrops and a large diversity of depositional environments throughout the basin. Three study transects were constructed by combining stratal geometries and facies observations into a high-resolution sequence stratigraphic framework. 3346 m of section were logged, 400 thin sections were studied, and 145 biostratigraphic samples were analysed for nannoplankton dates (Bassant, P., 1999. The high-resolution stratigraphic architecture and evolution of the Burdigalian carbonate-siliciclastic sedimentary systems of the Mut Basin, Turkey. PhD Thesis. GeoFocus 3. University of Fribourg, 277 p.).

The first transect (Alahan) is on the northwestern basin margin. Here, the siliciclastic input is high due to the presence of a river system. The siliciclastic depocentre migrates landwards during transgressions, creating an ecological window allowing carbonates to develop in the distal part of the delta. Carbonate production shuts down during the regression when siliciclastics return. The second transect (Pirinç) is also situated on the northern basin margin 12 km to the east of the Alahan section. It shows a complete platform-to-basin transition. An isolated carbonate platform complex develops during the initial flooding, which is drowned during a time of rapid sea-level rise and environmental stress, associated with prograding siliciclastics. The shelf margin then retrogrades forming large-scale clinoform geometries and progrades before a major sea-level fall provokes

* Corresponding author. Now at ChevronTexaco Energy Technology Company, San Ramon, California, USA.
E-mail address: Phil.bassant@chevrontexaco.com (P. Bassant).

0037-0738
doi:10.1016/j.sedgeo.2004.01.017

slumping collapse, followed by rebuilding of the shelf margin as sea level rises again. The third transect (Silifke) has a steep asymmetric Pre-Miocene valley-topography, forming a narrow strait, linking the Mut Basin to the Mediterranean. Strong tidal currents are generated in this strait area. Siliciclastic input is low and localised. Eighty metres of cross-bedded bioclastic sands are deposited in a tidal regime at the base. Subsequently, carbonate platforms backstep against the shallow-dipping northern flank, while platforms only develop on the steep southern flank when a firm wide shallow-marine substrate is provided by a bench on the footwall block. The energy of the environment decreases with increased flooding of the strait area.

Third-order sequences and higher-order parasequences have been identified in each transect and correlated between transects. Correlations were made using biostratigraphic data and high-resolution sequence stratigraphy in combination with the construction of the relative sea-level curve for each site. The third-order highstands are stacked in a proximal position and separated by exposure surfaces, while the lowstands, deposited in a distal setting, are separated by deep-marine (offshore or subphotic) deposits. The parasequences produce dominantly aggradational and progradational geometries with transgressive ravinement surfaces and exposure surfaces developing at times. Reconstruction of the depositional profile shows that the third-order sequences are driven by relative sea-level oscillations of 100–150 m, and that these may be attributed to 400-Ka orbital eccentricity cycles. The parasequences are driven by eustatic 20–30 m sea-level oscillations, which may be attributed to the 100-Ka orbital eccentricity cycles.

The isolated carbonate build-ups in the Pirinç and Alahan transects develop at the same time as bioclastic tidal deposits in the Silifke area during the transgression of sequence 1. This is caused by a difference in hydrodynamic regime: a direct result of basin morphology funneling tidal currents in the Silifke area. We also demonstrate how during the highstands a siliciclastic delta system progrades in the Alahan area, while only 12 km to the east, a fringing carbonate platform develops, showing how siliciclastic input can have a very localised effect on carbonate environments.

The exceptional quality of the outcrops with its variety of environments and its location at the Tethyan margin make this site a good candidate for a reference model for Burdigalian reef and platform architectures.

Keywords: Mut Basin; Sea level; Carbonate platform

1. Introduction

The rock record of the early Miocene of the Mut Basin in Southern Turkey shows an impressive diversity of carbonate and siliciclastic-dominated depositional environments (see map in Fig. 1). Excellent exposures of this early Miocene stratigraphic interval occur across the basin. Deposits formed in these diverse environments are found locally juxtaposed and also in different areas across the basin. They include high-energy tidal carbonate ramp deposits, fringing carbonate platforms with distinct margins and steep slopes, carbonate slumps deposited on the slope and in the basin, isolated carbonate build-ups, siliciclastic deltaic deposits, and siliciclastic fluvial deposits. Sezer (1970) described the isolated build-ups and the carbonate platform, and more recently, Gürbüz and Uçar (1995) briefly described the same build-ups in an abstract. Bizon et al. (1974) mentioned the slump deposits in a regional overview, Gedik et al. (1979) demonstrated the existence of a siliciclastic system in the dominantly carbonate-filled Mut Basin, and Eriş et al. (2004) described the stratigraphic organisation of the fluvio-deltaic system. The tidal carbonate deposits were first described as such by Bassant (1999).

This paper demonstrates the temporal and spatial relationship between these very diverse depositional environments and explains what happened to make these environments change. The nature of change is considered both temporally, as environments stack vertically in one location, and spatially, as distinct depositional settings develop coevally across the basin. The major factors influencing the depositional style were large relative sea-level rises and falls, the steep Pre-Miocene topography, and the nature of siliciclastic input. The time-stratigraphic framework developed shows that at least half the time contained within the studied interval is concentrated in discrete omission surfaces (both distal, proximal, and erosional temporal hiatuses).

In order to understand the depositional history of the study interval, three stratigraphic cross-sections

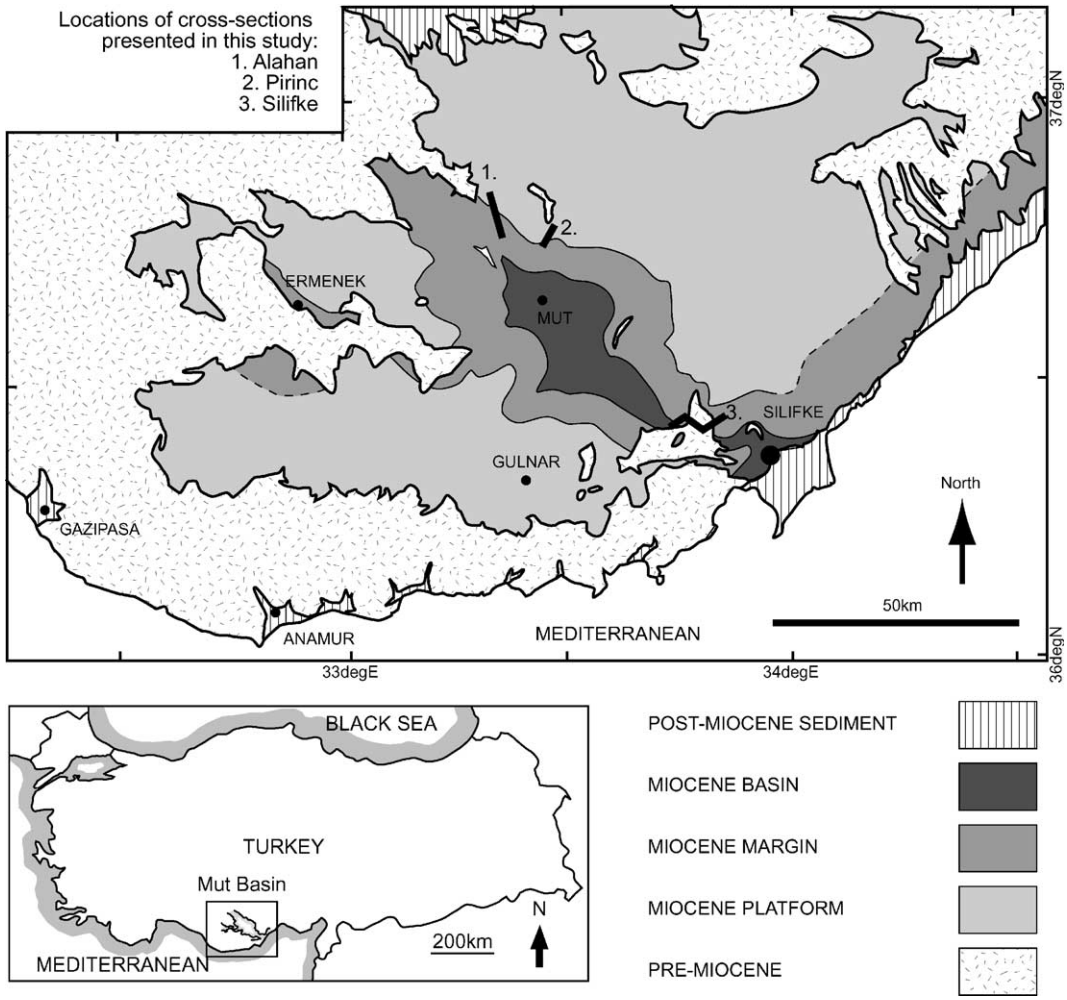

Fig. 1. Geological map of the Mut Basin (modified after Gedik et al., 1979). Showing major towns and villages and the locations of the three transects described in this study.

were constructed at key locations across the basin. Each cross-section was chosen to evaluate a different depositional setting. Biostratigraphic dating, sequence stratigraphic analysis, construction of relative sea-level curves for each cross-section, and mapped field relationships of the outcrops were used to correlate units between the different study sites. It was important to identify potential candidates for temporal hiatuses, inasmuch as these were often seen to correspond to packets of sediment in other locations. Once a time-stratigraphic framework had been developed, the evolution of basin-wide sedimentation patterns was described through time.

2. Geological setting

2.1. General tectonic history

The tectonic history of Southern Turkey, as concerns this study, can be summarised into three major periods:

(1) Late Palaeozoic to middle Eocene: formation of the Tethyan orogenic collage.
(2) Middle Eocene to middle Miocene: Tauride Orogeny during continued north–south convergence and collision; migration of deformation front south of Turkey.

(3) Late Miocene to recent: collision of Eurasia with the Arabic Plate (late Miocene) and start of the Neotectonic Regime.

(1) During the first period (Late Palaeozoic–middle Eocene), the Tethyan orogenic collage that now forms most of modern Turkey was created by complex north–south convergence. During this time, Tethyan continental fragments rifted from Gondwana in the south, drifted north across the Tethys, and were progressively accreted to Eurasia. The precise kinematic reconstruction is under debate: Robertson et al. (1996) summarise three alternative models, as proposed by Robertson and Dixon (1984), Dercourt et al. (1986, 1993), and Sengör et al. (1984), although in this study, the details that distinguish these three alternatives do not concern us. In the latest Palaeocene (?)–early Eocene (Sengör et al., 1985), collision started to occur along a northern branch of the Tethys, the Inner Tauride Ocean of Görür et al. (1984), and final closure happened in the late Eocene (Sengör et al., 1985) along the Pontide–Anatolide Suture, to the north of the Mut Basin.

(2) During the second period, as defined here, from the middle Eocene to the middle Miocene (Serravalian), continuing north–south convergence and general tightening of the orogenic belt characterised much of Southern Turkey, with the emplacement of the Lycian Nappes in the west continuing until the early Miocene. In the east, in the Adana Basin, thrusting may have continued until the middle Miocene (Williams et al., 1995). Northward subduction of remnant ocean crust to the south of Cyprus seems to have started in the early Miocene (Eaton and Robertson, 1993). The Arabian Peninsula in the east continued its northward movement, eventually colliding with Eurasia, along the Bitlis Suture Zone, in the Serravalian (Dewey et al., 1986).

Middle Eocene (Lutetian) platform carbonates are the last marine sediments to be found in Southern Turkey before the early Miocene. From middle Eocene to late Oligocene, the whole area was uplifted (Sengör et al., 1985). During this time, episodes of fluvial and lacustrine sedimentation occur in intramontane settings across most of the region (Yetiş et al., 1995). A diachronous marine transgression then floods the southern part of Turkey, starting from the south, in the late Oligocene in Cyprus, affecting the Mut, Antalya, and Adana regions during the early Miocene.

In the late Oligocene to early Miocene, the Mut Basin formed by approximate north–south extension within a mountainous terrain. The preextensional rock units that define the basin are made up of a complex orogenic collage formed during multiple phases of Tethyan closure. Kelling et al. (1995b) suggest that the crustal extension may be associated with orogenic collapse, leading to "trap door" subsidence. An alternative hypothesis is that the basin opened due to back-arc extension associated with the northward subduction of oceanic crust occurring in Cyprus around this time. This is consistent with the tectonic reconstruction proposed by Robertson (1998). During the Oligocene basin-opening phase, continental sediments were deposited, and it is only from the early Miocene that marine sediments, dominantly carbonates, appear. These are associated with the regional marine transgression and fill a mountainous preexisting topography as postextensional infill. The stratigraphic relationships are summarised in the stratigraphic column in Fig. 2. Fig. 3 is a topographic map of the preextensional "basement" or Pre-Miocene (as it will be referred to in this paper). This shows the approximate form of the Mut Basin during the early Miocene.

(3) The third phase in the tectonic history starts with the Eurasia–Arabia collision in the east in the Serravalian: it is this convergence that results in the westward expulsion of Turkey, along the North Anatolian and East Anatolian Faults, and is the start of the present Neotectonic regime (Sengör et al., 1985). The Anatolian Plateau is at this time uplifted by epeirogenic processes to its present elevation of 1–2 km above sea level. This induces a marine regression across the southern Turkey areas (Antalya, Adana, Mut, and Cyprus) from the Late Serravalian onwards, with deposition of Tortonian evaporites in the west and the south (Yetiş et al., 1995).

2.2. Climatic and faunal evolution of the Miocene Mediterranean Tethys

Throughout the Miocene, Tethyan ocean circulation patterns were controlled by the steady closing of the eastern end of the Mediterranean Tethys: the link between the modern Eastern Mediterranean and the

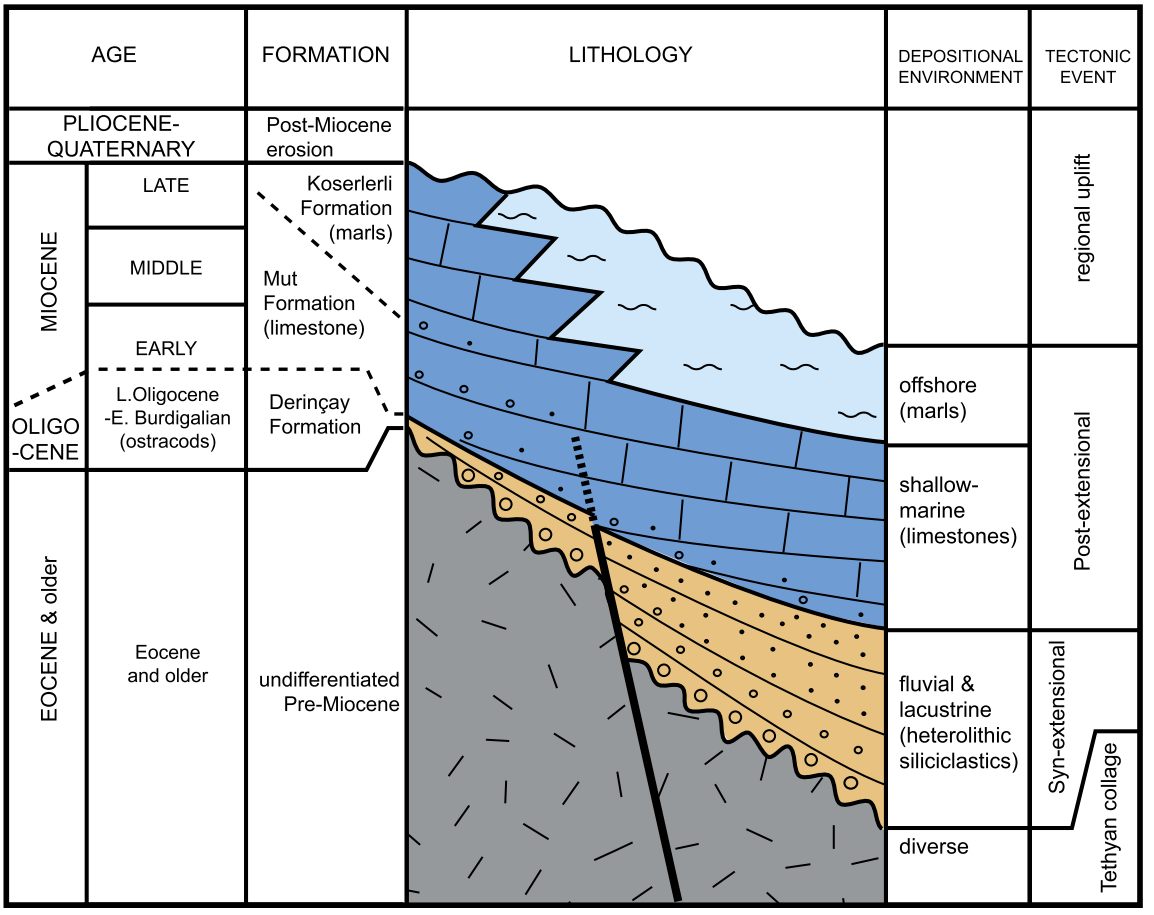

Fig. 2. Mut Basin lithostratigraphic column. This diagram focuses on the Miocene lithostratigraphy of the Mut Basin, as defined by Gedik et al. (1979). The Pre-Miocene is grouped into one unit.

Arabian Gulf. As the Arabian Plate converged on, and finally collided with the Eurasian Plate along the Bitlis Suture Zone, this passage was episodically shut off, being restricted in the Burdigalian, fully open in the Langhian, and closing finally in the late Miocene (Steininger and Rögl, 1984).

Fluctuations between different faunal assemblages at the scale of the Mediterranean Basin have been observed in the Miocene. These faunal assemblages are considered to be characteristic of climatic conditions. Foramol assemblages are associated with a temperate climate, rhodalgal assemblages with a subtropical climate, and coralgal facies with a subtropical to tropical climate. Observation of their variations in time at the scale of the Mediterranean Basin has allowed the reconstruction of Miocene climate change in this area.

It is in this context that Esteban (1996) describes the Mediterranean Neogene climatic evolution as follows: a middle Oligocene temperate climate in the Mediterranean Tethys was replaced by a tropical to subtropical climate during the late Oligocene, as indicated by the invasion of large benthic foraminifera that reached as far as the North Sea. Wide and deep seaways existed from the Indo-Pacific, via the Mediterranean to the Atlantic, and extensive coralgal–rhodalgal carbonates were deposited from Mesopotamia to the Mediterranean throughout the Aquitanian. The highest coral diversity of the Mediterranean Miocene occurred at this time. At the Aquitanian–Burdigalian boundary, the eastern end of the Mediterranean was closed off from the Persian Gulf, and the Mediterranean Tethys carbonates were limited to

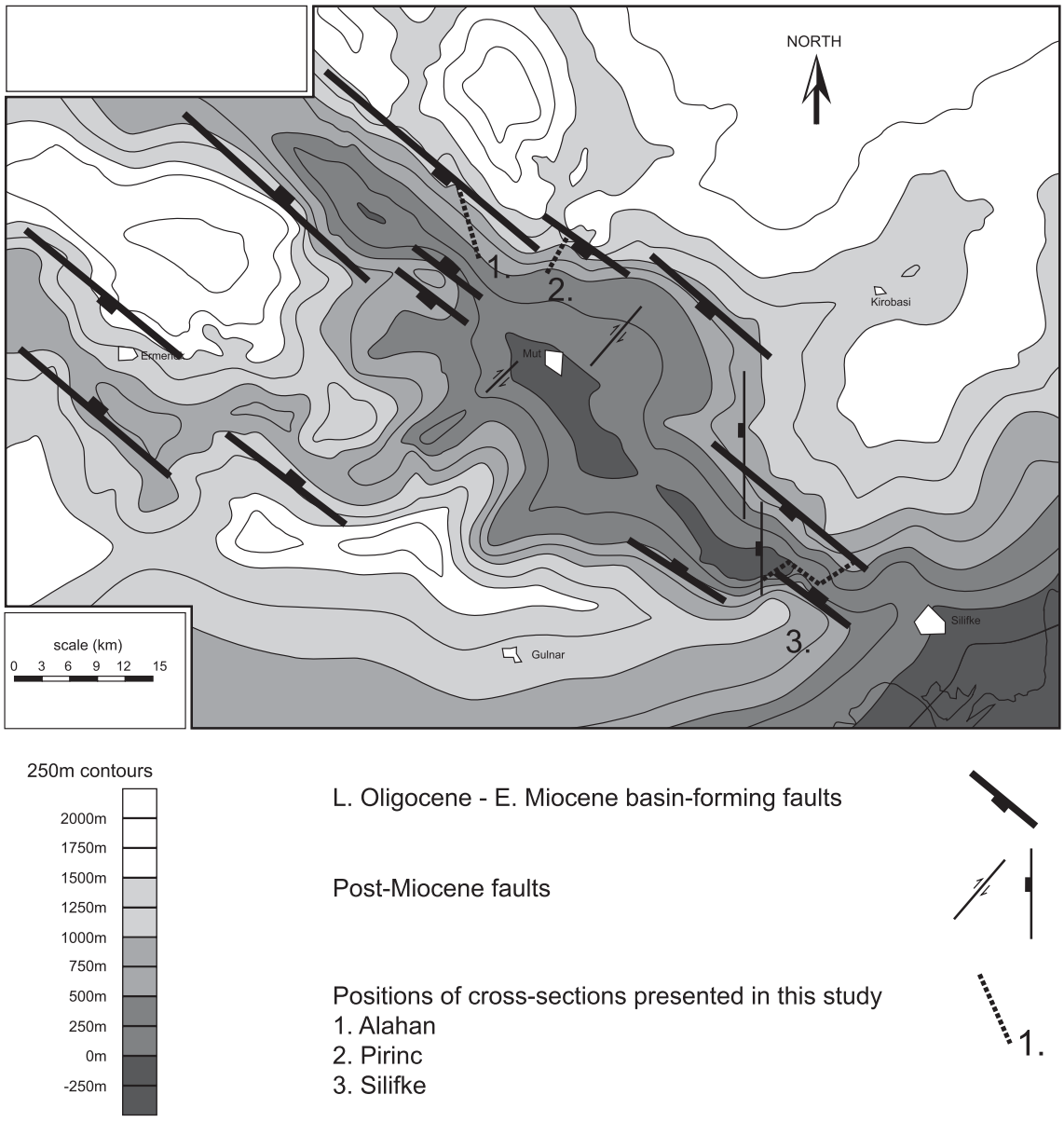

Fig. 3. Present-day Pre-Miocene topography (modified from Gedik et al., 1979). Includes also main structural trends of basin. We consider the form of the basin to have changed relatively little since the early Miocene, although the basin relief has probably been accentuated by basin-centre sagging. The basin fault distribution is interpreted by the current authors from a combination of mapped faulting (Gedik et al., 1979) and personal observations.

temperate rhodalgal–foramol types. This corresponds to a time of climatic deterioration and sea-level lowstand as proposed by Barron and Keller (1982), and also closure of the eastern end of the Mediterranean (Steininger and Rögl, 1984). The climate warmed in the Late Burdigalian–Langhian to tropical or subtropical conditions, once again permitting coralgal–rhodalgal carbonates to develop with moderate coral diversity (Esteban, 1996). This may correspond with the Langhian reopening of the seaway connecting the Mediterranean to the Arabian Gulf (Steininger and Rögl, 1984). Environmental conditions deteriorated in

the Serravalian due to apparent climatic cooling, and only impoverished subtropical to temperate carbonates are found in the western and middle parts of the Mediterranean region. The Late Serravalian saw a major global sea-level fall and uplift of the Turkish and Arabian Plates. The connection to the Arabian Gulf was finally closed. Corals survived in the Mediterranean from the Latest Serravalian to the Messinian. Then, during the Messinian, repeated major evaporitic draw-down resulted in interbedded thick evaporite deposits with fully marine deposits across much of the Mediterranean (Hsü et al., 1973).

According to Cavelier et al. (1993), the Late Burdigalian (early Miocene) was the warmest time of the Neogene, and it was considerably warmer than the current climate. As evidence, they cite the high northerly limits of tropical molluscan fauna and tropical carbonate shelf deposits as well as the distribution of terrestrial fauna and flora. They evoke a seasonal climate with contrasting semiarid and humid periods, the climate being too humid to deposit evaporites in the present desert areas such as the Sahara and the Arabian Peninsula. During this time, Southern Turkey was at roughly 35° of latitude, not far from its present position (Savostin et al., 1986; Yilmaz and Ozer, 1994; Westphal et al., 1986; Lauer, 1984). Making a direct comparison with the distribution of modern reefal fauna, such a high latitude would place the Mut Basin at the very limits of the coral growth area, and beyond that of Halimeda, in the zone of rare reef growth (Schlanger, 1981).

3. Previous studies of the Mut area

Surprisingly few published works exist about this area, considering the quality of the outcrop and the relatively large volume of work performed in the Adana Basin to the east and the Antalya Basins to the west. Marine transgression invaded a relict topography during the early Miocene in the Adana Basin (Schmidt, 1961), and this is a factor common to all three areas of Adana, Mut, and Antalya (Yetiş, 1988). Sezer (1970) in his thesis described the Miocene stratigraphy of the northern part of the Mut Basin, performed planktonic foraminifera dating, catalogued the Miocene macrofauna, and made a geological map. Bizon et al. (1974) observed a Neogene transgression (Burdigalian to Langhian, dated with planktonic foraminifera) in the Antalya, Mut, and Adana Basins. Gökten (1976) mapped out the Silifke area in the southeast of the basin, defining all the Phanerozoic units found. He placed major unconformities in the Carboniferous (Breton orogenic phase), in the Triassic (Palatin orogenic phase), astride the Jurassic–Cretaceous boundary (Ostervald orogenic phase), between the Cretaceous and the Eocene (Laramian orogenic phase), and between the Eocene and the Burdigalian (Helvetic orogenic phase). He defined five planktonic foraminiferal biozones in the Miocene limestones and marls, three of which are Burdigalian and the other two are Helvetian to Tortonian.

Gedik et al. (1979) mapped out the whole Mut Basin and revised the Phanerozoic stratigraphy. They also made a present-day structure map of the Pre-Miocene topography (see Fig. 3). Korkmaz and Gedik (1990) studied the source-rock potential of the Phanerozoic stratigraphy. Tanar and Gökçen (1990) provided a summary of the biostratigraphy of the Mut Basin. Kelling et al. (1995a,b) in two abstracts briefly describe the stratigraphy and tectonic setting of the Mut Basin, and Gürbüz and Uçar (1995) describe the existence of biohermal and biostromal reef bodies in the Mut Formation limestones of the Mut Basin. Schlaf et al. (1997) made an in-depth study of the molluscan assemblage of the Burdigalian in the Mut area, interpreting their environmental significance. Bassant (1999) studied the stratigraphic evolution of the Burdigalian across the basin, and it is a summary of this work that is presented in this paper. More recently, Pierre (2002) performed forward stratigraphic modeling of the Mut outcrops described in Bassant (1999), using the IFP's "Dionisos" modeling package. Additionally, a substantial amount of work was done in the middle Miocene of the Mut Basin (mostly Langhian) in the Ermenek area to the west (see the map in Fig. 1). This involved development of the detailed stratigraphic architecture (Janson, 1997; Janson and Eberli, 2000) and forward stratigraphic modeling of the Langhian outcrops (Broucke et al., 1998).

4. Methodology

This work is the result of a field-based study that took place over a period of three years (1996–1999),

Table 1
Facies summary table

Facies	Description	Fauna and flora	Diagnostic features	Processes	Energy of environment	Interpreted depositional environment
1	Coralgal framestones	Diverse coral, encrusting red algae	In situ corals and red algae	Constructed	Medium	Clay-free platform–slope
2	Muddy coralgal framestones	Diverse coral, encrusting red algae	In situ corals and red algae in clays	Constructed	Medium–episodically low	Platform–slope
3	Coralgal floatstones	Diverse coral, encrusting red algae	Coralgal debris in finer matrix	Pseudoautochthonous debris	Medium–low	Platform to constructed gentle slope
4	Muddy coralgal floatstones	Diverse coral, encrusting red algae	Coralgal debris in finer clay-rich matrix	Pseudoautochthonous debris	Low	Platform to constructed gentle slope
5	Rhodolithic float-bindstone	Red algae as rhodoliths	Dominance of rhodoliths	Autochthonous growth or allochthonous accumulation (currents or gravity)	Medium–episodically high	Sediment starved platform–slope
6	Muddy rhodolithic float–bindstone	Red algae as rhodoliths	Dominance of rhodoliths in clay-rich matrix	Autochthonous growth or allochthonous accumulation	Medium–episodically high	Sediment starved platform–slope
7	Microbial coralgal boundstones	Small corals, encrusting red algae, encrusting forams, sponges, oysters, barnacles	Presence of encrusting foraminifera, sponges, microbial micrites with fenestrae	Autochthonous growth	High	Platform top
8	Oyster rud–boundstones	Oysters, red algae, Serpulids, barnacles	Dominance of oysters	(1) constructed, (2) pseudoautochthonous debris	?	Restricted platform–slope
9	Soritid grain–packstones–wackestones	Soritids, red algae, diverse molluscs, echinoids	Soritids common	Allochthonous–pseudoautochthonous detrital carbonates	Low	Very shallow-restricted platform
10	Miliolid grainstones–packstones	Miliolids, (Nummulitids, Amphisteginids, Soritids), red algae, molluscs, echinoids	Miliolids common	(1) transport and sorting by traction currents, (2) slope gravity flow	Medium	Shallow platform

11	Nummulitid grain packstones	Nummulitids, Amphisteginids (Miliolids, planktonic forams), red algae, molluscs, echinoids	Nummulitids and Amphisteginids common	(1) transport and sorting by traction currents, (2) slope gravity flow, (3) pseudoautochthonous accumulations	Medium	Platform–slope
12	Planktonic foram micropackstones/marls	Planktonic forams (Nummulitids) infaunal echinoids	Planktonic forams and infaunal echinoids abundant	Planktonic accumulation	Low	Slope–basin
13	Coralgal rudstones	Corals red algae, Amphisteginids, Nummulitids	Sorted coralgal debris	Pseudoautochthonous–allochthonous debris	Medium–high	Platform–slope
14	Bryozoan grain–rudstones	Bryozoans, red algae, molluscs, Amphisteginids	Well sorted, dominance of bryozoan debris	Allochthonous detrital carbonates	high	Intersubtidal
15	Slump deposits		Extensive rigid and plastic deformation	Allochthonous gravity flows	Variable	Slope–basin
16	Continental gravels–muds	(stromatolites)	Red colour, absence of marine fauna	Allochthonous	Variable	Fluvial–lacustrine
17	Littoral-shallow sublittoral muds–silts	Diverse molluscs	Presence of shallow marine molluscs in clays and silts	Allochthonous	Low	Littoral–sublittoral
18	Coquina rudstone	Diverse thick-shelled molluscs	Diverse molluscan debris with heterolithic basement gravels	Pseudoautochthonous–allochthonous	Medium–high	Foreshore–upper shoreface
19	Marine conglomerates	Large echinoids (Clypeaster), oysters, other molluscs	Heterolithic basement conglomerates with marine fauna and cement	Allochthonous	High–medium	Foreshore–upper shoreface
20	Marine sands–calcarenites	Diverse molluscs	Heterolithic basement sands with marine fauna	Allochthonous	Medium	Upper–lower shoreface
21	Marine silts–muds	Planktonic forams and pteropods	Silts–muds with pteropods and planktonic forams	Allochthonous	Low	Shoreface–offshore

This table summarises the descriptions and interpretations for the 21 facies used in this paper.

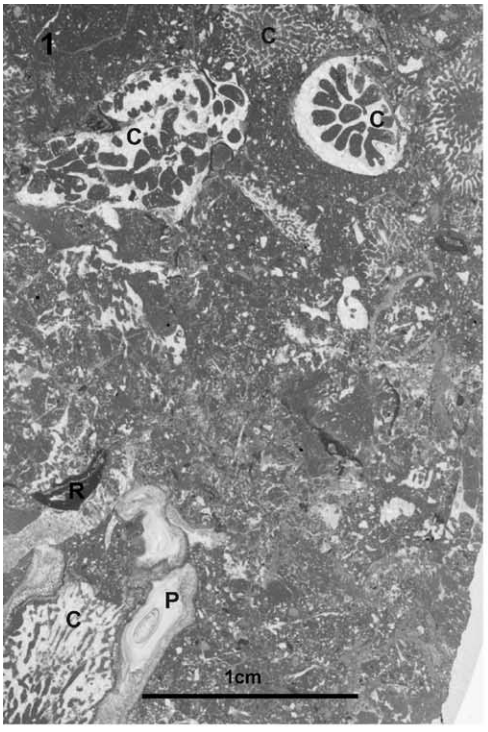
1
C
C
C
R
C
P
1cm

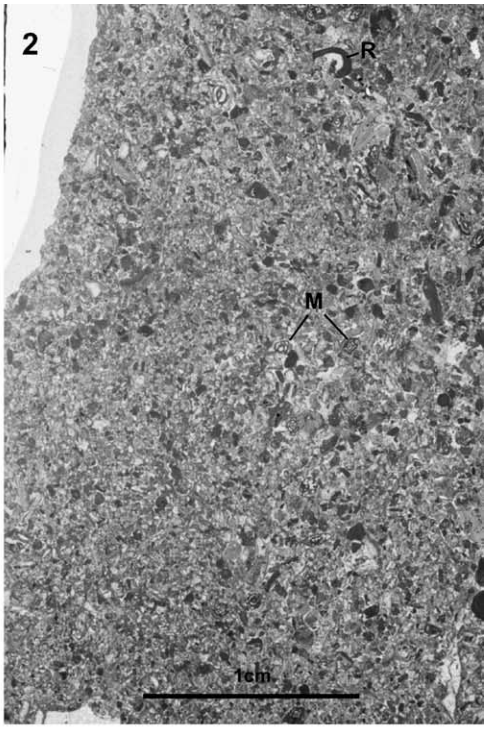
2
R
M
1cm

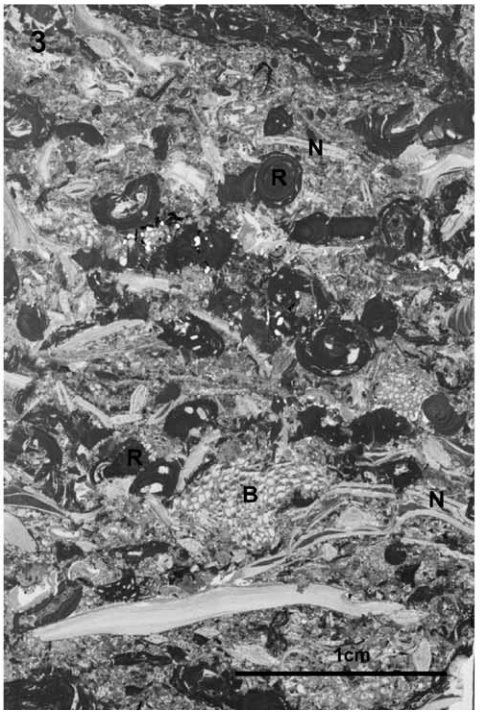
3
N
R
R
B
N
1cm

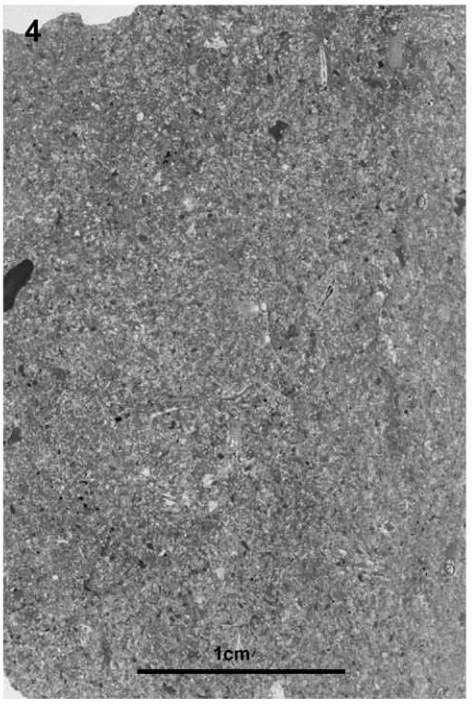
4
1cm

with a total of five field expeditions of 4–8-weeks duration each.

4.1. General work-flow

The methodology applied in this study is as follows:

(1) Geological mapping: during the initial reconnaissance, the geology of two broad areas of interest (total of 800 km^2) was mapped, and specific locations were chosen for detailed study. The field mapping was built on previous maps made of the area (Sezer, 1970; Gökten, 1976; Gedik et al., 1979) by adding information about the Miocene stratigraphic organisation, including the biostratigraphic dating. The aim was to place areas chosen for detailed study within a more general stratigraphic context.
(2) Descriptions of bedding geometry: the bedding patterns of areas chosen for detailed study were examined, and sedimentary packets were defined. These packets are partially bound by surfaces and possess a characteristic internal bedding geometry. This was done in the field from sketches and photographs and in the office from photographs. It was important to return to the field to reassess the geometries described as the understanding of the outcrop progressed. Field measurements of length, height, and angle were made across the outcrop.
(3) Facies descriptions: measured sedimentary logs were made at key areas on the outcrop. Thicknesses were carefully measured in order to accurately reconstruct the outcrop. Facies were analysed, identified, and classified. To help in this facies analysis, samples were studied in thin section. A semiquantitative approach was opted for, in which the relative abundances of the important faunal elements were given a value from 1–5, 5 being the most abundant and 1 being simply present. The microfacies were documented by scanning (in positive transmitted light) the complete thin section: this had the advantage of illustrating the centimetre-scale sedimentary textures found. The nature and importance of different types of surfaces were recognized. Shallowing and deepening trends were identified in the logs, and this defined shallowing/deepening sequences of different scales.
(4) Construction of stratigraphic cross-section: the geometrical and facies information were then combined to define sequences and parasequences, and a stratigraphic cross-section of the outcrop was constructed showing the facies distribution, the bedding patterns, and the positions of the sequence boundaries.
(5) Feedback: the construction of the stratigraphic cross-section involved the assessment and comparison of large amounts of data, and an iterative convergent process is implicitly applied to arrive at the best-fit solution for the definition of sequences and the integration of the different data sets into a coherent story. This often involved a reexamination of the data and the outcrop.

4.2. Biostratigraphy

Nannoplankton was principally used to date the sections: the dating was performed by Carla Müller (IFP, Paris) on 145 samples. Ages were defined using the nannoplankton stratigraphy of Martini and Müller

Fig. 4. Facies photos (1). These 4 microfacies photos are whole thin-section photos (positive light) from the isolated platform Kizil Kaya outcrop. Exact positions of samples are shown in the log in Fig. 8. Photo 1 is a muddy coralgal floatstone (facies 4) from the aggrading phase of parasequence 1b. P indicates Pelecypod fragments, C indicates coral fragments of diverse kind, and R indicates rare fragments of coralline red algae. Photo 2 is a medium, sorted Miliolid grainstone (facies type 10, see Table 1) belonging to the prograding upper section of parasequence 1b. Diverse Miliolid forams are common (M), and coralline red algae is an abundant constituent of the sediment (R). Photo 3 is a coralgal rudstone (facies 13). Red algae (R), bryozoa fragments (B), and Nummulitid Foraminifera—typical of the slope environment (N)—are abundant in this sample. These sediments are part of the progradation of parasequence 1d and consist of a mixture of platform top and slope sediments deposited on the slope in a prograding clinoform packet. Photo 4 is a micropackstone (facies 12) characterised by a fine grain-size and the presence of a planktonic and Nummulitid Foraminifera assemblage. These are typically deposited below wave-base in the lower photic to subphotic zone.

(1986), which attributes 1.7 million years to the NN4 nannoplankton zone, being the interval of interest in this study. Basinal marls were ideal for this dating, and many slope deposits such as fine packstones also contained sufficient nannoplankton to determine an age. For each data point, a relative abundance of nannoplankton was determined in order to qualify the validity of the information. Also, planktonic foraminifera were dated by Roland Wernli (University of Geneva, Switzerland) on 10 samples. Ages were determined using the foraminifera stratigraphy in Bolli et al. (1985). Biozones N7 and N8 are observed in these samples. Observations were made by the Institute of Palaeontology in Vienna (W. Piller, pers. com.), concerning the molluscan biostratigraphy of two of the study areas (Pirinç and Alahan, see later), and these corroborated the other dating methods. Details of the biostratigraphic analysis can be found in Bassant (1999).

4.3. Sequence stratigraphic framework

A sequence/parasequence nomenclature has been used to designate the two scales of sedimentary cycle described in this study. "Sequence" is used to indicate large sedimentary cycles (probably third-order) of

Fig. 5. Facies photos (2). Photo 1 shows a muddy coralgal framestone (facies type 2; Table 1) with large domes and plates of highly bored corals (mostly Porites) surrounded by clay-rich muds. These are deposited in a shallow marine environment with periodic or episodic inputs of fine-grained terrigenous siliciclastic material. Photo 2 shows a rhodolithic float-bindstone (facies type 5) from the top of the Kizil Kaya isolated platform. This facies is interpreted as being deposited during a rapid flooding that leads to the drowning of the platform. Photo 3 shows a clean coralgal framestone (facies type 1) directly overlying a marine conglomerate (facies 19). The transition is an abrupt flooding of a shallow marine fan delta into a reefal system, with carbonate producers colonizing the fan-delta top. Photo 4 shows the microbial coralgal boundstones (facies type 7) from the upper part of an isolated platform. This is a very hard, highly cemented rock with 20–40 cm spaced bedding partitions. Corals and red algae are present but never grow to greater than 2–10 cm. Encrusting organisms are the main sediment generator. These include bryozoans, sponges, foraminifera, and unidentified microbial encrusters.

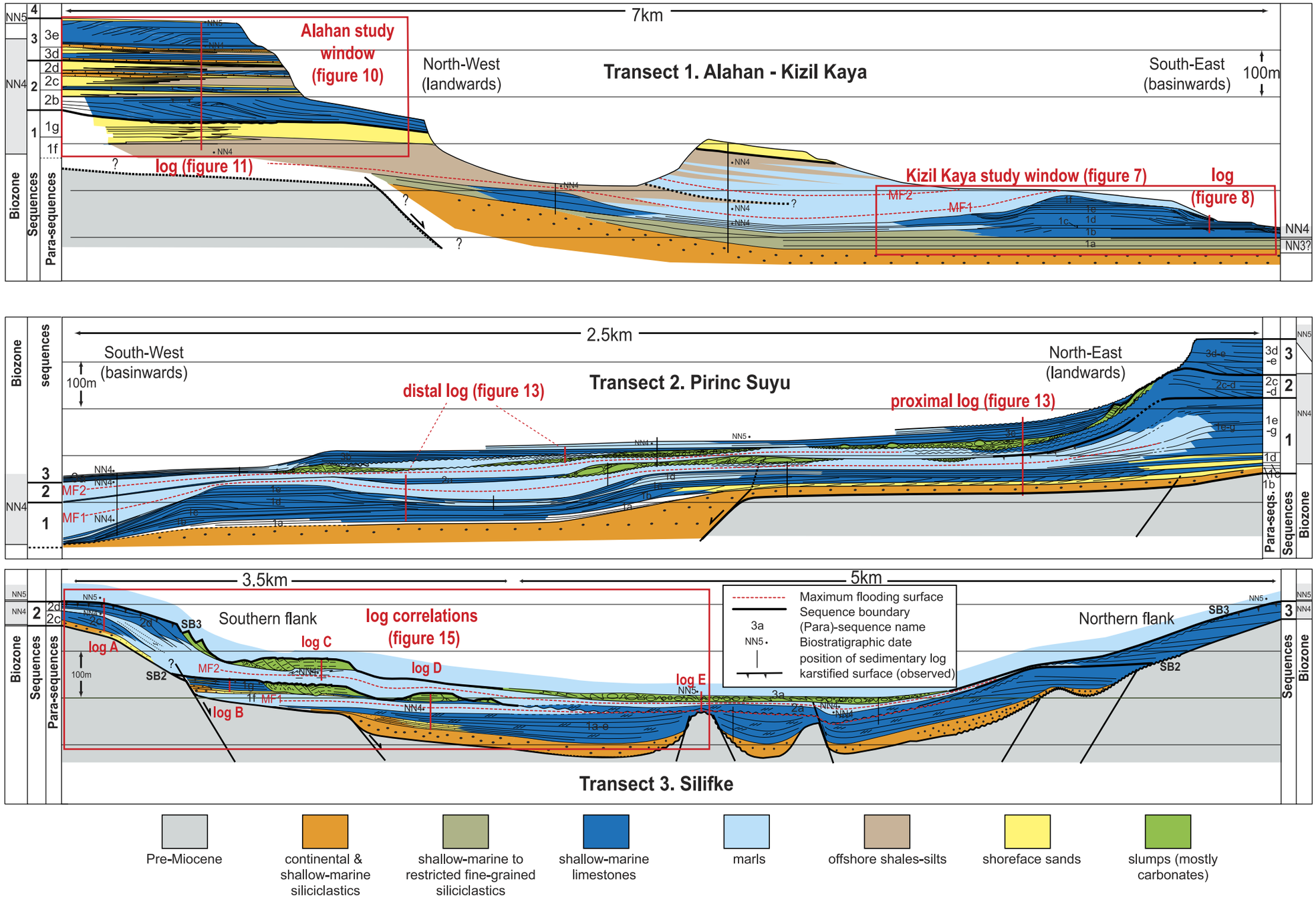

Fig. 6. Three cross-sections of principle study areas. This figure shows the three transects from the key study sites across the basin. The transects are all at the same vertical scale, although the horizontal scale differs. An appropriate datum has been chosen for each transect to reconstruct as best as possible the depositional geometries. The sequences and parasequences are labeled accordingly (SB—sequence boundary; MFS—maximum flooding surface).

approximately 50–100 m thickness. These are labeled sequences 1 to 4, with SB1 to SB4 denoting the sequence boundary and occurring at the base of each sequence of the same number. Sequence boundaries show evidence for important platform-top exposure and a significant basinward shift of sedimentation across the sequence boundary. They are broken down where possible into lowstand (LST), transgressive (TST), and highstand systems tracts (HST). The lowstand and transgression are frequently difficult to distinguish from each other because the carbonate response to increased flooding is often increased local productivity. "Parasequence" denotes the smaller sedimentary cycles (probably 4th–5th-order) of approximately 10–30 m thickness. Parasequence boundaries (PSB) typically show poor or no evidence of exposure and may often simply be abrupt flooding surfaces. Parasequence architecture mostly shows periods of aggradation at the base followed by periods of progradation at the top. The turn-around from aggradation to progradation is not formally defined by systems-tract nomenclature for this scale of cycle. In this paper, the term relative sea level is used to mean the sum of eustatic sea level and subsidence (whether due to tectonic activity or compaction of the underlying sediments).

5. Facies

The facies described in the field from the logging of measured sections and from facies mapping of outcrops have been classified into 21 facies types. This classification is based on sedimentary textures, sedimentary structures, and faunal content observed in the outcrop and from the microfacies analysis. The facies classification developed and applied in this study is functional, inasmuch as the study of the facies per se is not the primary goal here. Facies descriptions use the nomenclature defined by Dunham (1962), as modified by Embry and Klovan (1971) for describing constructed reefal facies. The carbonate facies defined here and their distribution along the depositional profile are similar to those described by Goörür (1994) in the Karaisali Formation (early Miocene) of the Adana Basin. The facies are summarised in Table 1 and illustrated in Figs. 4 and 5.

6. Depositional history of the Alahan–Kizil Kaya transect

The Alahan–Kizil Kaya transect (transect 1) shown in Fig. 6 was constructed by correlating the detailed study sites of Alahan and Kizil Kaya using mapped field relationships. Details of this correlation are discussed in Bassant (1999).

Kizil Kaya is located in the Mut area approximately 14 km to the northwest of Mut town (see Fig. 1). The outcrop is two vertical cliffs, which form a right angle. A detailed stratigraphic cross-section of this outcrop is shown in Fig. 7. Fig. 8 presents one of the sedimentary logs made here and illustrates its position relative to the stratal architecture of the platform. Illustrated on this log is a stratigraphic transition from a littoral siliciclastics system, through a shallow marine carbonate platform, slope, and finally deep-water marls. Photographs of Kizil Kaya are shown in Fig. 9: the top photo is an overview, while the lower photo is a detail showing the depositional geometries from the logged area featured in Fig. 8. The eastern cliff that runs approximately north–south and faces west is 500 m in length, while the northern cliff, running east–west, can be traced out over 1.5 km. The two cliffs meet near the highest point, which is a little less than 100 m high. This site was studied because it presents a 3D outcrop of one of the isolated platforms of the Mut Formation in the Mut area. Fourteen sedimentary logs were made at the base and on the flanks, while the cliff face was sampled by abseiling down the north face near the junction with the eastern face.

The Alahan study area is 21 km to the north–west of Mut town, just beneath the main road leading from Mut to Karaman, after passing the Alahan village and the Alahan monastery access road, in the Karaman direction (see Fig. 1). The Alahan valley cuts in a southeasterly direction through the northern flank of the Mut Basin escarpment. The Alahan detailed study area stratigraphic cross-section (Fig. 10) is constructed from outcrop observations on both sides of the valley. This transect is constructed from (a) a sedimentary log through the complete interval, (b) bedding pattern observations coupled with spot facies observations, and (c) detailed facies mapping. Fig. 11 is a

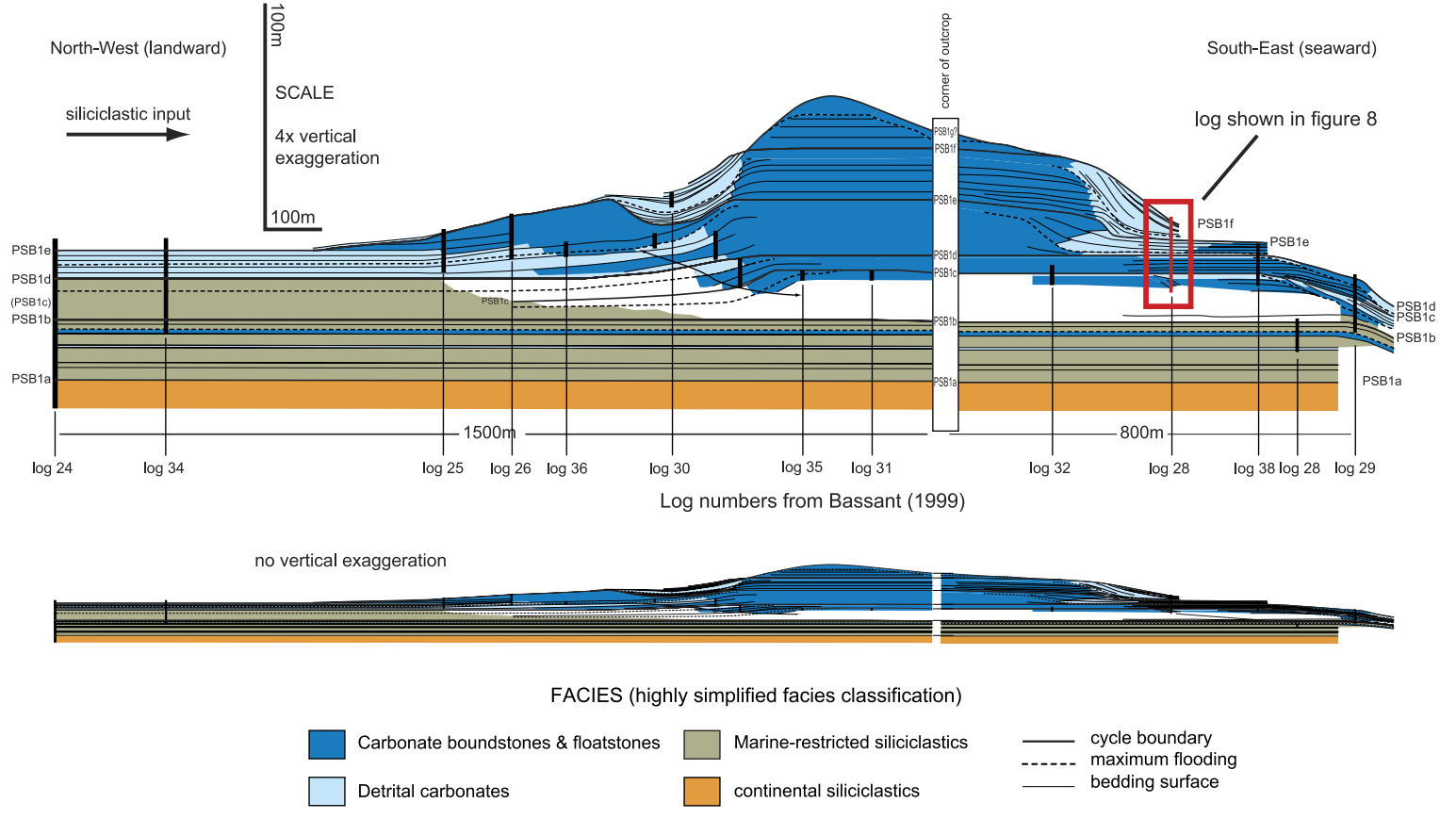

Fig. 7. Kizil Kaya stratigraphic cross-section (facies and geometries). This diagram shows the details of the bedding geometries and a simplified facies distribution of the Kizil Kaya platform, part of the Alahan–Kizil Kaya transect.

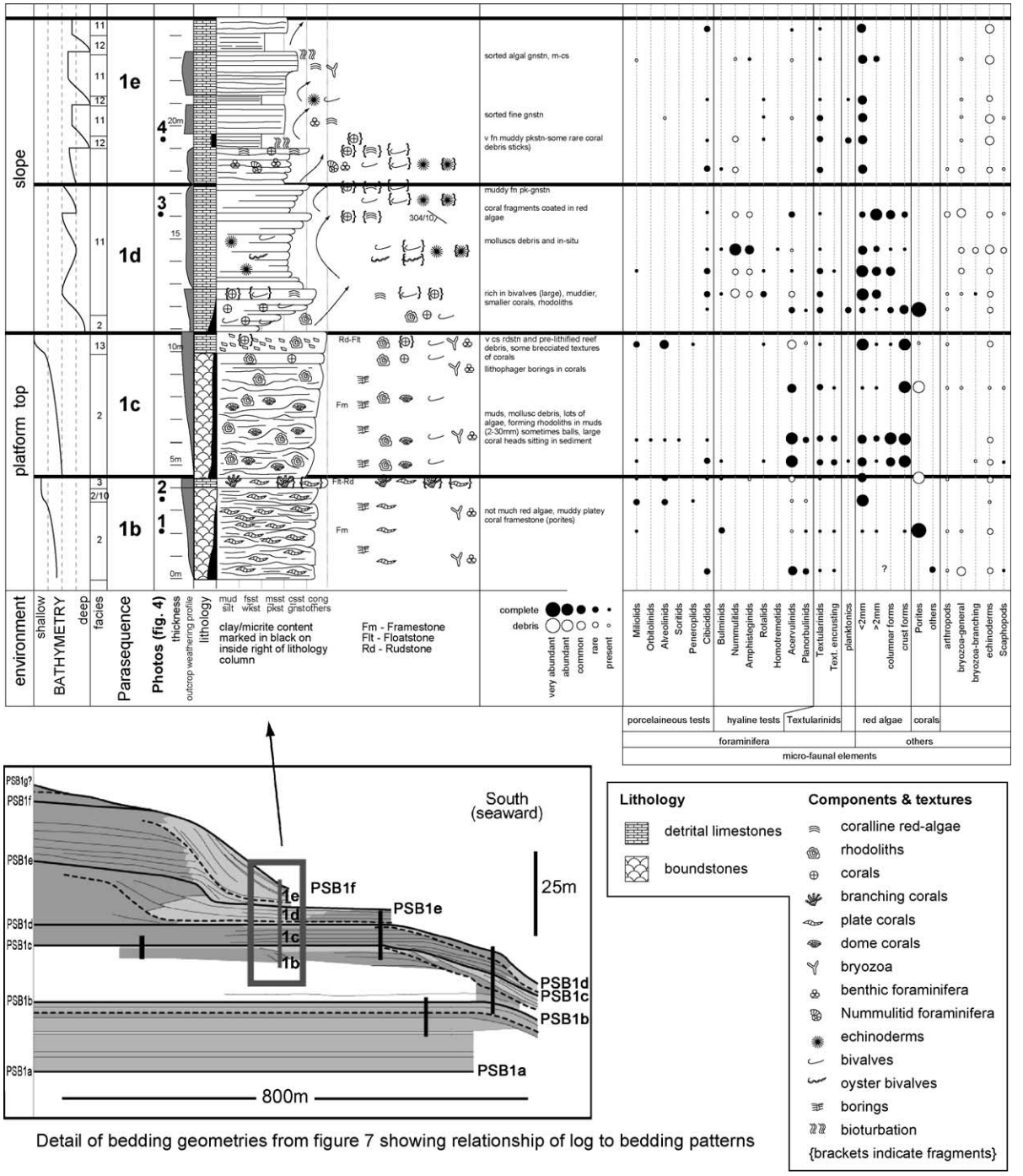

Detail of bedding geometries from figure 7 showing relationship of log to bedding patterns

Fig. 8. Kizil Kaya log. This is from the southern edge of the platform. It shows the vertical facies trend and its association with the trend in bedding geometries (bedding architecture detail is taken from Fig. 7). The positions of the facies illustrated in Fig. 4 are indicated (1 to 4). Above parasequence boundary 1d, a major backstepping event occurs, and the platform-size contracts, placing sediments in this log above parasequence boundary 1d on the platform slope.

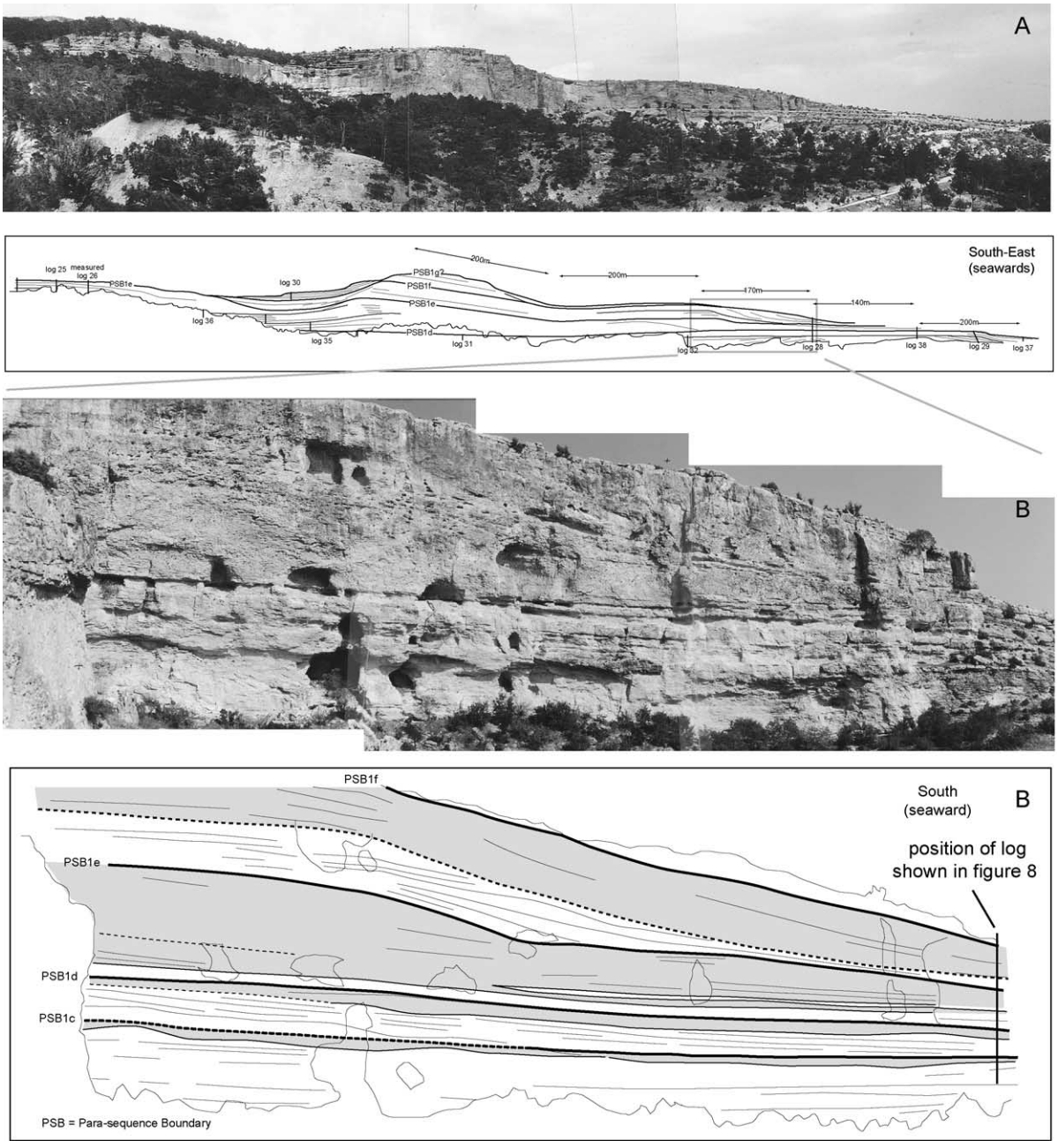

Fig. 9. Kizil Kaya photographs. Photograph A shows a general overview of the Kizil Kaya build-up. Photograph B shows a detail of the stratal architecture of the eastern flank of Kizil Kaya, with the location of the log from Fig. 8 indicated. This photo covers approximately the same interval as the bedding geometries inset in Fig. 8.

summary log through the whole Alahan section, while Fig. 12 shows three photographs of the outcrop. The middle photograph is an outcrop overview, while the top and lower photographs show details of the depositional architectures discussed below in the text.

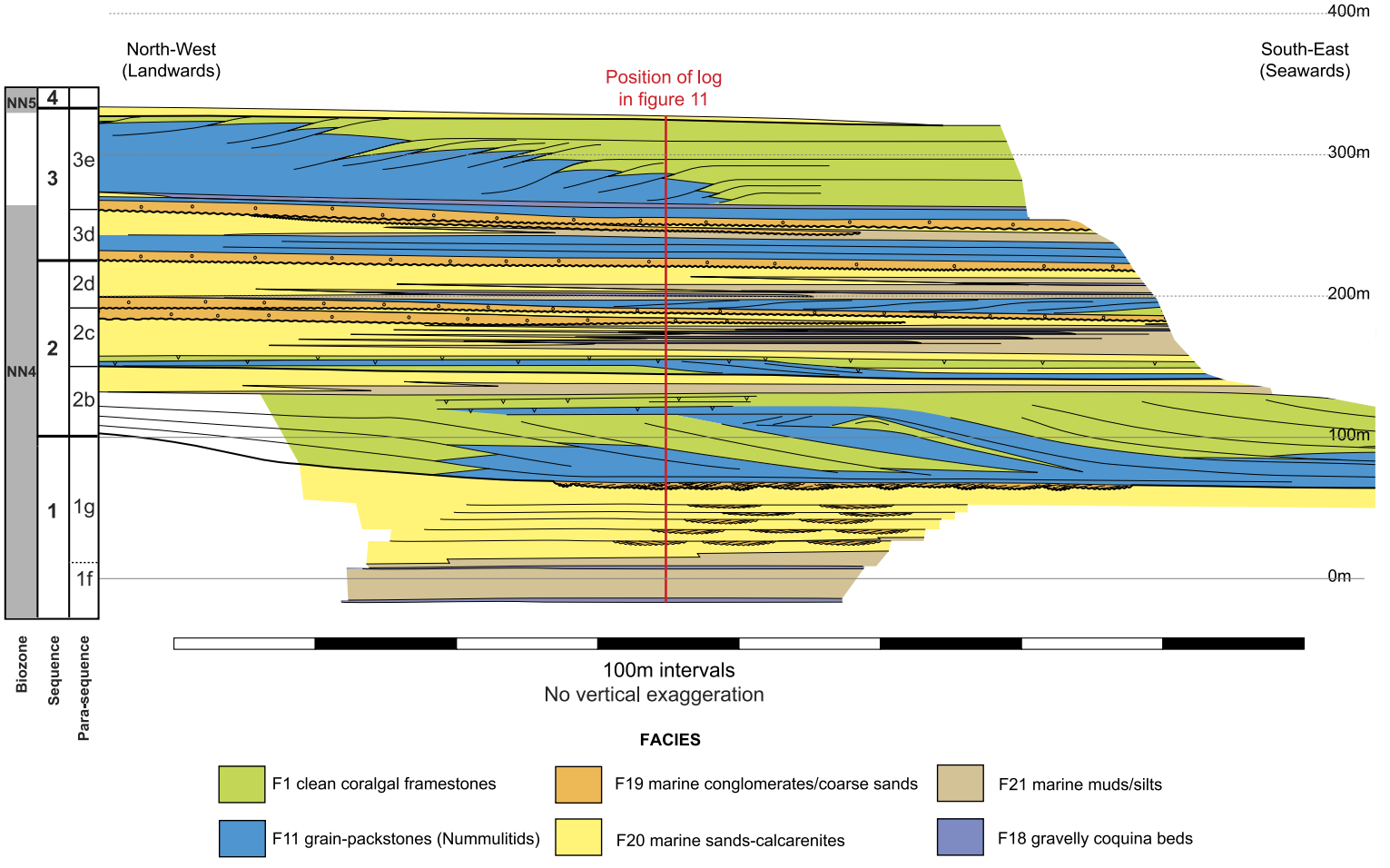

Fig. 10. Alahan stratigraphic cross-section (facies and geometries). This shows the complex interbedding of shallow-marine siliciclastics and carbonates in the shallow shelf environment. Cyclicity occurs on at least two different scales, and it is this superposition of scales of cycle that create the apparent architectural complexity of the system.

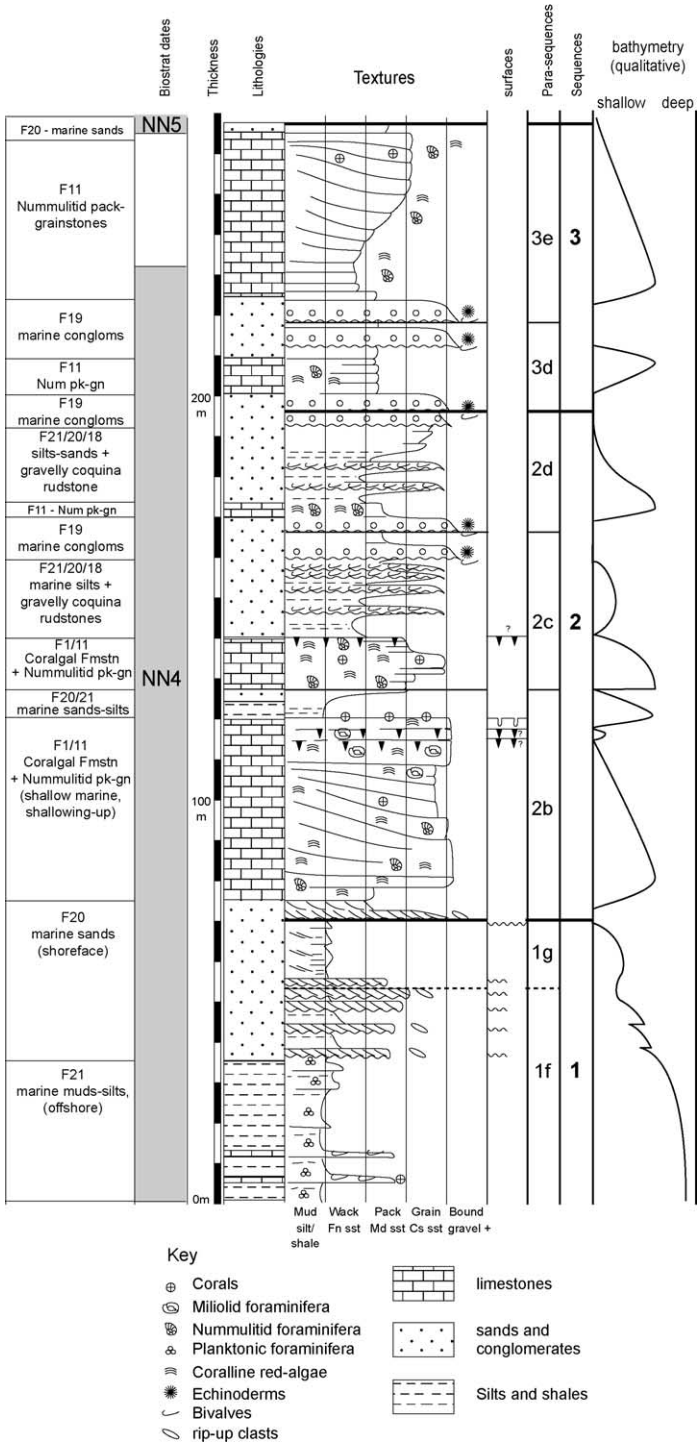

Fig. 11. Alahan log. This log shows the evolution of the proximal platform in the Alahan area. Its location is indicated on Figs. 6, 10, and 12.

6.1. Sequence 1

Sequence 1 is Late Burdigalian in age. It lies within the NN4 nannoplankton biozone. One sample in the lowest marine sediments (from a marginal marine–estuarine environment) suggested an NN3 biozone, although this was inconclusive. Throughout sequences 1–3, a river system (the Paleo–Goksu) delivers mud-dominated terrigenous sediment from the northwest corner of the basin. Marine flooding of the basin-floor during sequence 1 progressively forces the siliciclastic depocentre to retreat to the northwest.

6.1.1. Transgression 1 (parasequences 1a–e)

Initially in parasequence 1a, continuous beds of mud-dominated estuarine clays rich in molluscs are deposited. As flooding continues, low-relief carbonate banks develop contemporaneously with the deposition of estuarine clays between the banks (parasequence 1b). The bank observed in Kizil Kaya (Figs. 7–9) is 20 m thick and 1000 m in length, with the flanks dipping at 5°–8°. Facies in the bank during the transgression of parasequence 1b are mostly clay-rich coralgal framestones and floatstones (facies 2 and 4). The progradations of parasequence 1b fill out the flanks of the mound on the seaward (southeast) and landward (northwest) sides, with deposits on the top of the mound being thin to absent. On the seaward side, toplap is observed in the prograding wedge. The prograding units on the landward side are composed of muddy coralgal floatstones, while on the seaward side, they are dominantly Miliolid grainstones (facies 10), grading distally into Nummulitid grain-packstones (facies 11). The top of the progradation is defined as the top of parasequence 1b (i.e., PSB1c). It shows toplap and renewed transgression above. As the long-term flooding trend of sequence 1 continues, the low-relief carbonate banks develop into isolated platforms, and the siliciclastic depocentre retreats to the northwest. Parasequence 1c continues to have fine-grained siliciclastics deposited in the off-platform position (see Fig. 7): parasequence boundary (PSB) 1d marks the top of siliciclastic deposition in the Kizil Kaya area, with the transgression of parasequence 1d seeing the retreat of the siliciclastic depocentre west to a more proximal position closer to its source (the Paleo-Goksu River that feeds in from the northwest). Throughout the deposition of parasequences 1c to f, the Kizil Kaya isolated platform area is progressively reduced, and the general trend is that of retrogradation. However, the internal architecture of each parasequence is clearly defined by a repeating motif of aggradation then progradation: these progradations do not compensate for the overall retrogradational trend. Aggradation occurs at the base, while towards the top of each parasequence, strong progradational geometries develop, depositing sediment on the flanks of the isolated platform, often with local beveling of the underlying platform-slope, and toplap geometries at the parasequence top. The platform sediments are mostly coralgal framestones and floatstones (facies 1–4) in parasequences 1c and d, while in parasequences 1e and f, microbial coralgal boundstones (facies 7) are deposited on the platform. This switch to a microbial-dominated platform top is probably a response to some kind of environmental stress leading to nonideal conditions for coralgal growth. Potential causes are numerous, but the most likely candidates are increased water turbidity and nutrient content due to an encroaching delta system or a climatic cooling. Deposition on the platform flanks occurs mostly during the progradations of the parasequences and consists dominantly of detrital carbonates (Miliolid and Nummulitid grainstones of facies 10 and 11). Some evidence for exposure exists on the platform-top at the parasequence boundaries, but sampling/logging of the platform top is limited. The evidence is strong dissolution along fractures observed in hand-specimens, and increasing trends of this dissolution upward towards parasequence boundaries with less dissolution directly above the boundaries. The observed toplap at the parasequence boundaries on the prograding flanks indicates a forced regression at times, and while this is no evidence for actual exposure, it suggests it is likely. The top of the platform is characterised by an abundance of rhodolithic floatstones and bindstones, deposited during the final drowning event, as the platform passed into the subphotic zone during drowning.

6.1.2. Highstand 1 (parasequences 1f and g)

The sequence description continues in the Alahan detailed study window shown in Fig. 10. Here,

parasequences 1f and g are aggrading to prograding siliciclastics of the deltaic system. Parasequence 1f is mostly offshore silts and fine sands with some thin carbonate beds, while parasequence 1g are offshore silts and sands, shallowing to shoreface sands, with tidal channels developing in the top of the parasequence, containing large amounts of gravel and coarse sand. The top of this coarse siliciclastic unit is sequence boundary 2. It is the top surface of the most proximal packet, overlain by carbonates of sequence 2,which deposited during transgression.

6.2. Sequence 2

Sequence 2 is Late Burdigalian in age (NN4 nannoplankton biozone). In the Alahan area, it occupies a very proximal position compared to the other transects, and no lowstand is deposited in this area.

6.2.1. Transgression 2 (parasequence 2b)

The lowest parasequence observed in sequence 2 is parasequence 2b (Fig. 10). This is because the Alahan area was exposed while parasequence 2a was being deposited elsewhere. By the time the Alahan area was flooded, the transgressive trend of sequence 2 was well underway, and flooding occurred rapidly, probably explaining the rapid switch from a tidal siliciclastic to a carbonate environment. Parasequence 2b is 55 m thick and consists of a set of prograding carbonate clinoforms 40 m thick overlain by 10 m of coarsening-up siliciclastics (see Fig. 10). The facies are described in the log in Fig. 11. The progradations of parasequence 2b can be seen in the lower photograph in Fig. 12. The bedding geometries of the clinoforms are very distinct. Oblique tangential clinoforms are observed prograding in a southeasterly direction, with slopes of up to 20°. Toplap is common. The clinoforms are organised in lobes or tongues a few hundred metres across, and they nest around each other as they prograde to fill up flush to the platform top surface, creating a grossly tabular platform geometry that is internally partitioned by the lobe boundaries. These geometries are interpreted as the result of a relative sea-level stillstand, while a shallow wide platform area produces sufficient volumes of carbonate sediment to prograde. The sediment in the carbonate clinoforms is mostly red algae and corals. Sedimentary textures vary between autochthonous and paraautochthonous textures (bindstone, framestone, and floatstone: here grouped together under the facies 1) and detrital carbonate (grainstones and packstones). Siliciclastic sand is abundant (up to 50% of sediment) in the lowest 8 m of the carbonates and is present throughout the clinoforms but in small quantities (<2%). It is mainly fine, well-sorted heterolithic sands. The corals in the autochthonous textures are always small Porites (<10 cm), with platey and knobby morphologies: the red algae have a fundamental role in stabilising the sediment, forming thin mats interbedded with small coral colonies. Judging from the fragmented nature of the corals and algae, transport followed by renewed growth seems to be common processes in this environment, hence the use of the term “paraautochthonous. In the detrital packstone and grainstone textures, Nummulitid and Amphisteginid foraminifera are very common. These are typical of a slope environment. Miliolid foraminifera are only seen in the top few metres of this platform. A number of distinct features are observed 2 m below the top of the carbonate clinoforms packet: siliciclastic basement pebbles up to 5 cm in size are found mixed with the carbonate sediment as well as a sharp surface with minor autobrecciation and ferruginous infill below. This may indicate an exposure event. The top of this platform is abrupt: it is a coral-encrusted surface with overlying silty clays. The encrusted nature of the platform top indicates flooding and demise of carbonate production, probably due to the arrival of clays and silts. These clays form the base of a 10-m thick coarsening-up siliciclastic unit. These change upward into medium-grade sands over 10 m, with some carbonate-rich intervals. This is interpreted as a shallowing-up trend from lower shoreface–offshore silts to upper shoreface sands.

6.2.2. Highstand 2 (parasequences 2c and d)

The parasequence boundary (2c) is placed at the top of the underlying shoreface sands at the surface where sands are overlain by carbonates. This picking strategy is also applied to PSB2b–2d and SB3 and thus requires some commentary. The mixed system described in Alahan (Fig. 11) contains good candidates for parasequence boundaries in both the

siliciclastics and the carbonate intervals. However, because a clastic–carbonate pair make up one cyclic unit, they could not both form parasequence boundaries. The clastic candidate for a parasequence boundary is the top of a coarsening-up shallowing-up offshore to shoreface trend, terminating in coarse foreshore fan-delta deposits: the parasequence boundary (PSB) is placed at the top of this trend (at the base of the topmost fan delta, which is considered to be deposited during initial flooding of the next parasequence). Exposure surfaces are often found close to the top of the carbonate units, just prior to demise of carbonate productivity. We have systematically placed the PSB at the top of the shallowing-up siliclastics for 2 reasons:

(1) The shallowing clastic trend is the stronger indicator of the net balance between sediment input and relative sea level, with shallowing-up clastics showing long-term regression, more so than a single minor exposure surface in the carbonates.
(2) Carbonate growth is a response to the clastic signature: the carbonates develop during times of transgression in which a window of opportunity is created for carbonate production. The carbonate response is to rapidly produce and locally fill up, then track sea level. This makes it sensitive to higher frequency relative sea-level fluctuations and rapid periods of exposure. Such short exposure events are less significant stratigraphically than long-term shallowing and deepening of clastic facies.

Parasequence 2c is 42 m thick. The lower 12 m of the parasequence is a shallow-marine carbonate unit, and this is overlain by approximately 30 m of siliciclastics starting as coarse sand at the base, fining rapidly up over 2 m, then coarsening up gradually from silts punctuated with gravelly coquina beds (estuarine deposits) to coarse sands and finally gravels and conglomerates at the top. The conglomerates are deposited in a shallow marine environments probably as fan deltas, and constitute the most proximal deposits. Coralgal framestones form the base of the carbonate unit, while the top half is red-algal grainstones containing abundant Nummulitid foraminifera. The top surface of this carbonate unit is autobrecciated and infilled with coarse siliciclastic sands. Laterally, the surface is red-stained over corals and conglomerates. This surface has been interpreted as a karst (autobrecciation), marine hardground (encrustation and red-staining) and flooding surface (distal shift of overlying facies), similar to the top of the carbonate unit in the parasequence below (parasequence 2b). The thickness of the carbonate unit in parasequence 2c varies from 12 m in the log to 1 m westwards in the most proximal outcrop, and seaward prograding geometries are observed. When the beds are followed laterally seaward, the single karstified surface on the top of the platform bifurcates into two karstified surfaces separated by siliciclastic sands, and gravelly sands and conglomerates then overlie this topmost surface. This suggests the karstification process is controlled by high frequency cyclicity beyond the resolution of the parasequences considered here. Parasequence 2d is approximately 30 m thick. The lower 12 m of this parasequence is a reefal carbonate unit which thins rapidly landwards and has landwards prograding bedding geometries. These directly overlie the coarse fan-delta conglomerates of parasequence 2c. The transition from the conglomerates to carbonates at parasequence boundary 2d occurs rapidly across a sharp surface: coral framestones sit in direct contact on the conglomerates. Some pebbles and sand grade siliciclastic material are reworked into the base of the carbonate beds, but this quickly diminishes to nothing. The carbonate unit is organised as follows: over the first 5 m, diverse types of dominantly dome corals give way to almost monospecific platey Porites morphotypes, then the framestones are replaced by Nummulitid pack-grainstones rich in red-algal debris. This change in coral morphology from domes (middle reef front; James, 1984) to plates (lower reef front) and final loss of corals seems to reflect an environmental deterioration for the growth of corals, including a possible reduction in incident light. Laterally, the platform thickness varies rapidly: in the log (Fig. 11), only 2 m of platform are found. The upper 18 m of the parasequence is a coarsening-up siliciclastic unit trending from marine clays and silts directly over the carbonate unit to coarse fan-delta conglomerates at the top of the sequence. Gravelly, coquina beds are common and occur cyclically throughout the siliciclastic interval. Sequence boundary 3 is placed at the base of the conglomeratic fan delta deposits (facies 19).

This surface may be a major erosion and by-pass surface. The sequence boundary is placed specifically at the base of the gravel beds because we interpret that the overlying conglomeratic interval is deposited during initial floodback. Other similar conglomeratic intervals occur above and below, but we choose this one as the major sequence boundary because of the stacking patterns: this is where the siliciclastic sands and conglomerates are thickest (i.e., most seaward position of facies belts preserved here) and where the carbonate units are thinnest. Additionally, this is where the fan-delta conglomerate beds are most amalgamated (see Fig. 11), indicating the most significant regression. Stacking patterns can at times be misleading (due to lateral variability of sediment thickness and type), so we acknowledge that one parasequence boundary above and below this sequence boundary constitute good alternative candidates for the sequence boundary position.

6.3. Sequence 3

Sequence 3 is Late Burdigalian to Langhian in age. Most of the sequence is in the NN4 (Late Burdigalian) nannoplankton biozone, and the first NN5 (Langhian) sample appears in the sands at the top of parasequence 3e. It is comprised of two parasequences in the Alahan area. These have been correlated basin-wide as sequences 3d and 3e, with 3a–c not deposited in this area due to exposure.

6.3.1. Highstand 3 (parasequences 3d and e)

Parasequence 3d is approximately 21 m thick. It has a very similar organisation to parasequences 2c and d: a 10-m thick carbonate unit develops at the base overlying the fan-delta conglomerates of the sequence below. The carbonate sediments consist mainly of sandy Nummulitid packstones and grainstones (facies 11), with no constructed facies observed. This platform is in turn overlain by 4 m of coarsening-up sands topped by a 7-m conglomeratic package. Parasequence boundary 3e is at the top of these conglomerates. Parasequence 3e is Late Burdigalian (NN4 biozone) to Langhian (NN5 biozone) in age, and is approximately 45 m thick (laterally variable). The highest NN4 biostratigraphic sample is found with this parasequence, and the lowest NN5 sample is found in the sands at the top: the sample positions are shown in the log in Fig. 11. The carbonate unit at the base of this parasequence is a 40 m-thick carbonate platform (see top photograph in Fig. 12). At the base of this carbonate unit are 5 m of relatively tabular sandy shelly packstone and grainstone carbonate beds (facies 11), above which reefal carbonates develop. The reefal facies were examined in the field, and the back-reef deposits were logged. A variety of coralgal boundstone textures form the platform, while coarsening- and cleaning-up fine Nummulitid packstones and wackestones form the back-reef deposits. Initially, production is localised in a seaward position; the beds aggrade then "prograde out in a landward direction (backfilling). A thin siliciclastic interval of medium shelly sandstone containing some gravel directly overlies this platform. It contains rare nannoplankton, and this is the first NN5 date found in this section. Sequence boundary 4 is placed at the top of these sands.

7. Depositional history of the Pirinç transect

The Pirinç Suyu study site is 10 km due north of Mut. It consists of a valley 1.4-km deep cutting into the northern escarpment of the Mut Basin, gouged out by the passage of the Pirinç River which descends from the Anatolian plateau in the north before joining the Goksu River in the south. The valley is sufficiently deep (1500 m of relief) to provide excellent exposure from the Mesozoic basement to the Miocene. The steep irregular valley sides are punctuated by vertical cliff faces. This geomorphology permits the observation of bedding patterns and the physical correlation of bedding surfaces from basement onlap to basinward lapout within the Miocene. The basement structural organisation is also clearly visible. Logs have been taken within the Miocene sediments in order to construct the stratigraphic cross-section.

The Mesozoic basement is a grey highly faulted Mesozoic limestone (Lower to Middle Triassic, Gökten 1976; Cretaceous; Sezer, 1970), bound by a Palaeocene erosional unconformity and overlain by Tertiary (possibly Eocene?) dolomitised limestone, which has a highly karstified top surface. Normal faults, now with a strike of 110°–120°, dropping down to the south, are activated during the basin-

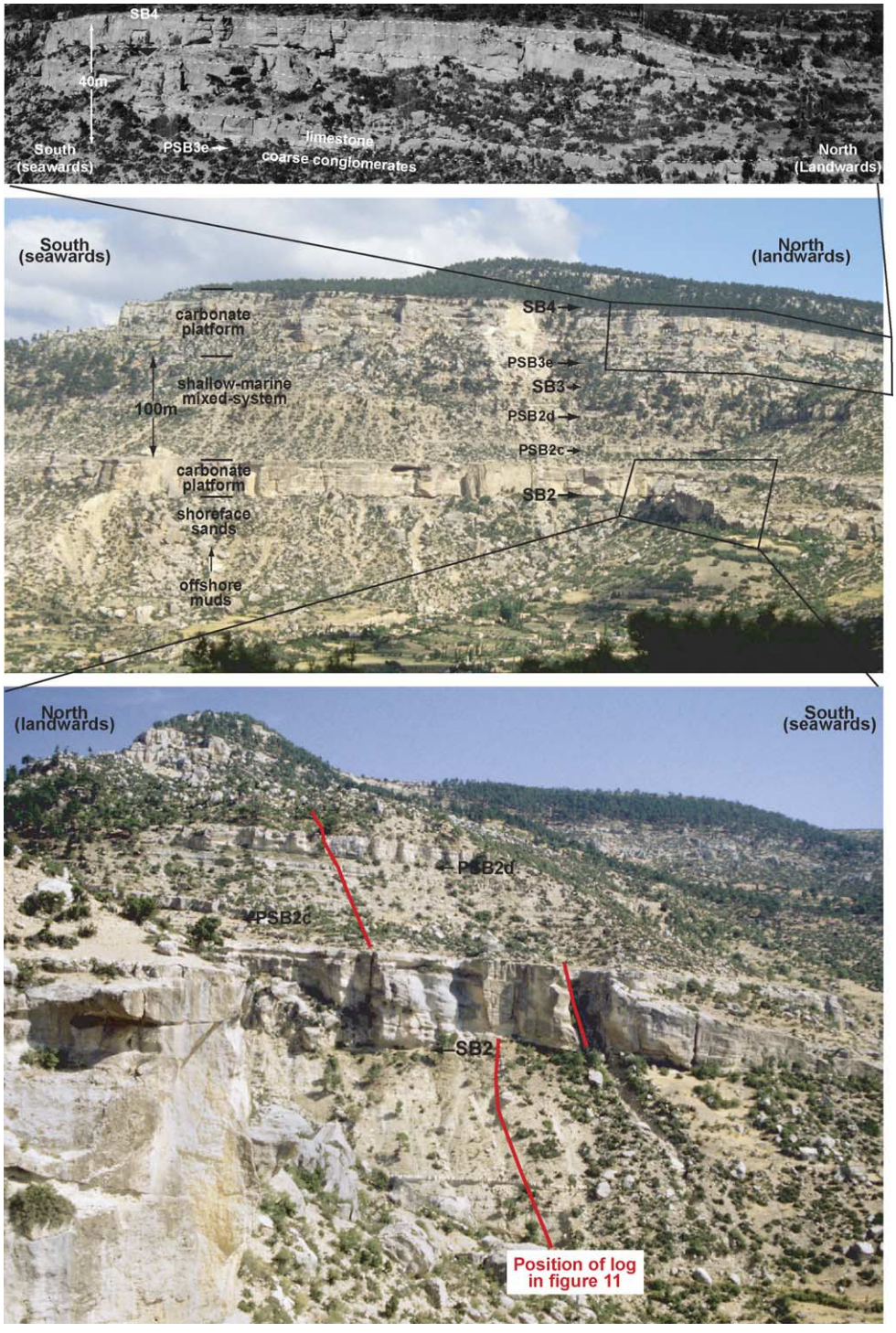

Fig. 12. Alahan photographs. The top photograph shows parasequence 3f in which a carbonate bank progrades in a landward direction ("backfills") to fill in a lagoon area behind. The middle photo is an overview of the Alahan study site, with the sequence boundaries indicated, and the bottom photograph shows the prograding geometries of parasequence 2b.

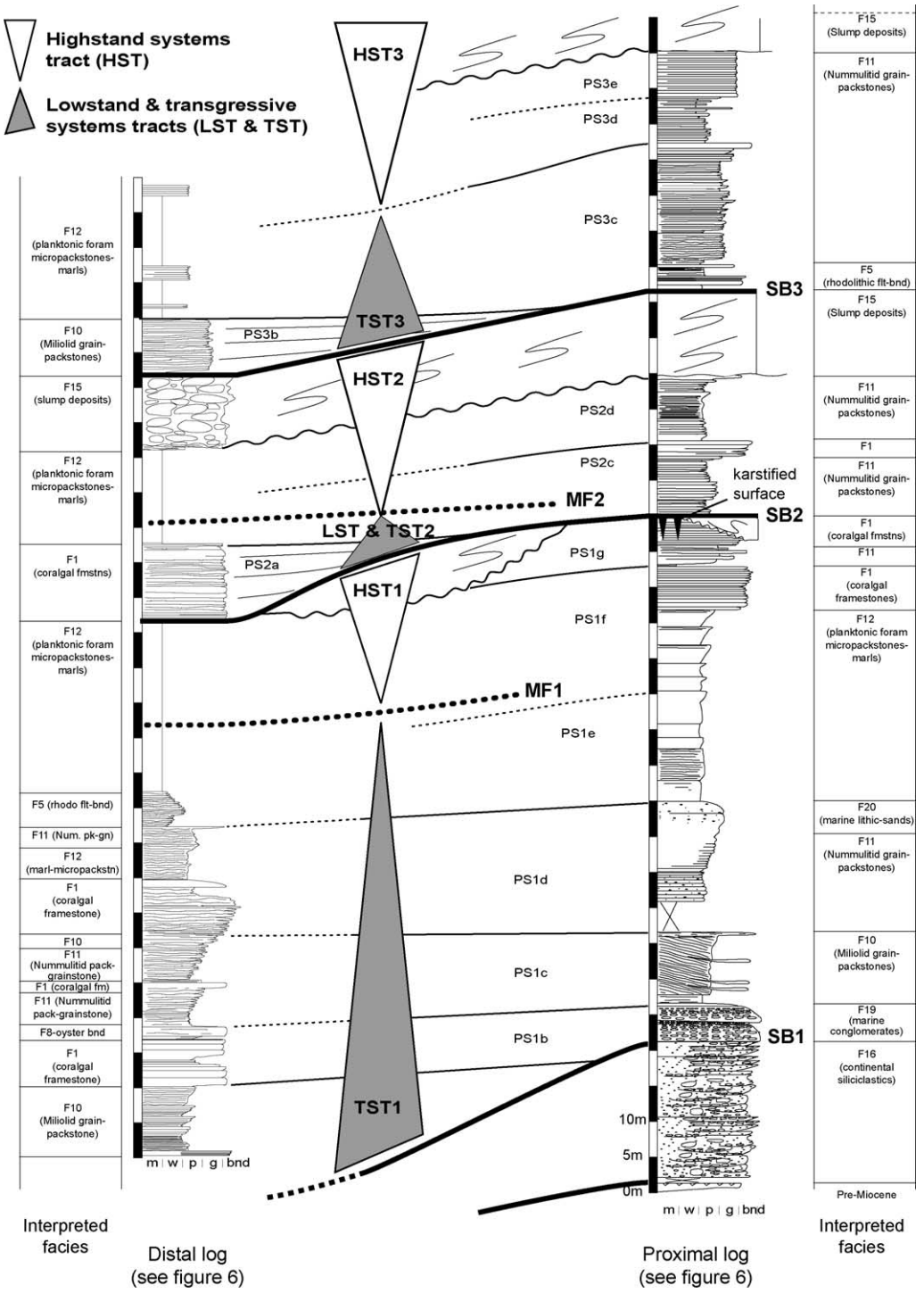

Fig. 13. Pirinç logs. The log on the right describes the proximal setting, while the log on the left describes the distal setting.

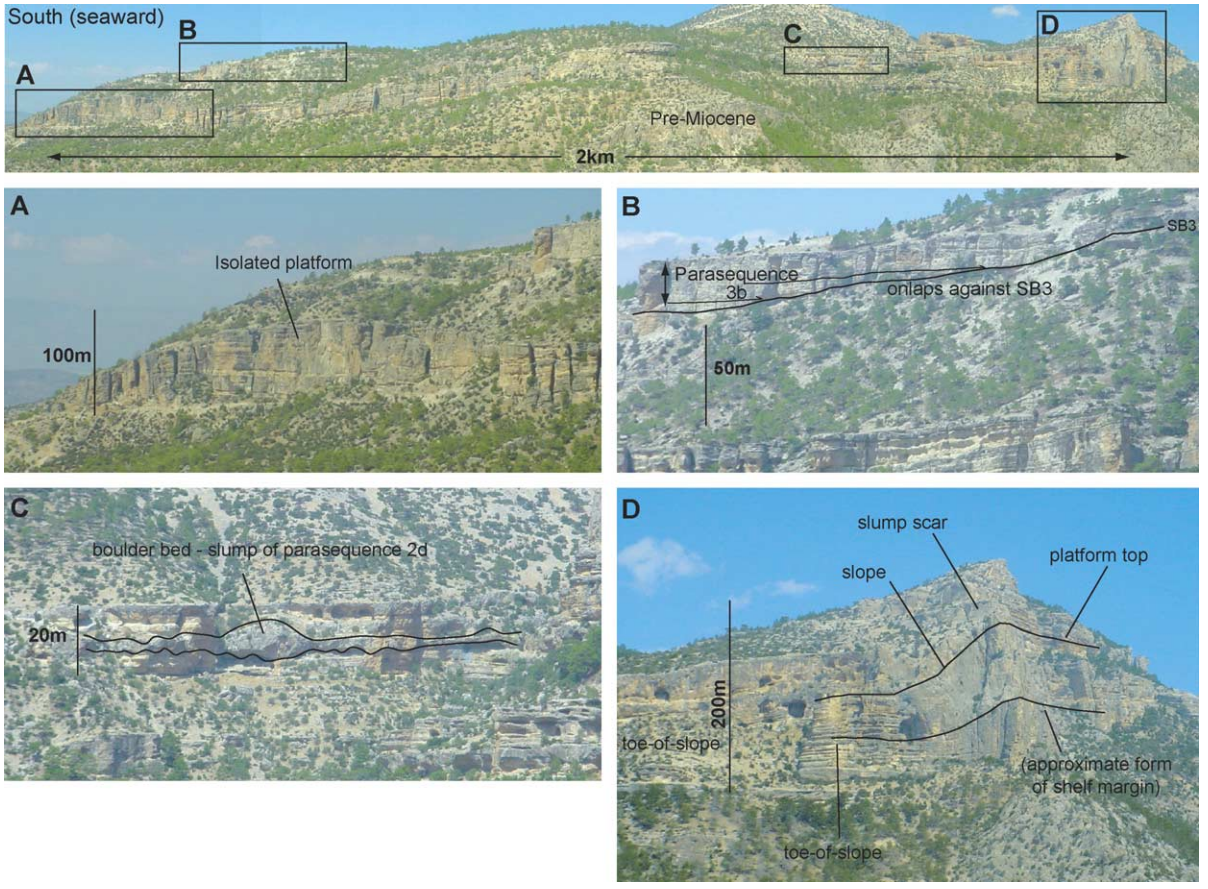

Fig. 14. Pirinç photographs. The top panel is an overview panorama of the complete Pirinç outcrop showing the platform-to-basin transition. The basin-centre is to the left of the photo (south). Inset A shows the isolated platform that develops in a basinward position during the transgression of sequence 1. Inset B shows parasequence 3b, a carbonate fringing platform deposited during transgression against the underlying sequence boundary 3. It is overlain by deep-water marls and underlain by marls and distal slump deposits. Note the onlapping geometries onto the underlying surface. Inset C shows a boulder bed of the parasequence 2d slump packet at the foot of the platform slope. Inset D shows an oblique view of the steep-sloping shelf margin. The platform top and slope are sketched in to illustrate the form of the margin. The updip limit of one of the slump scars (corresponding to SB3) is also indicated.

opening phase in the Oligocene. The synextensional sediments are the continental clastics of the Derinçay Formation and have been logged in this study. They pinch out as coarse conglomeratic alluvial fans against the preextension basement in the north and thicken to the south to fill the 110°–120°-trending graben structure with over 250 m of fluvial and lacustrine sediment. The Miocene marine carbonates are first deposited during the Late Burdigalian. These carbonates are considered as post extensional deposits, inasmuch as they are almost undeformed by the basin faulting. However, some small faulting does occur that shares the same strike as the basin faults: a normal fault offsets the Miocene carbonates by 3 m over the crest of a faulted basement block. It is sealed by the first slump unit in the Burdigalian study interval. This may be a small readjustment of the basement fault, or it may be the result of differential compaction of the underlying continental Derinçay Formation over the crest of the footwall block below. Fig. 6 (centre panel) shows the reconstructed stratigraphic cross-section for the Pirinç area. Fig. 13 shows a log correlation between the toe-of-slope and the distal platform, illustrating the facies relationships and the sequence architecture. Fig. 14 is a set of outcrop photographs illustrating the diverse deposi-

tional architectures. Throughout the following descriptions, continual reference is made to the transect in Fig. 6.

7.1. Sequence 1

7.1.1. Sequence boundary 1

Sequence Boundary 1, the base of sequence 1, lies somewhere within the fluvial sediments of the Derinçay Formation and beneath the first marine flooding. These fluvial sediments were not studied in detail as part of this work, but a complete description of the Derinçay Formation stratigraphic architecture can be found in Eriş et al. (2004).

7.1.2. Transgression 1 (parasequences 1a–e)

At the start of the first sequence (parasequences 1a–c) during early transgression, relatively tabular strata gradually onlap the gently sloping basement topography as accommodation space is created. A variety of facies are found, with coralgal boundstones building a gently sloping relief on the seaward extremity of the carbonate platform, bioclastic sands in the internal areas of the platform, and some siliciclastic sediments, sourced locally (no major river system is found in this area), in the most proximal areas near the onlap with the basement. The parasequences in the proximal area are organised into prograding packets, formed as the shoreline deposits. As the rate of creation of accommodation increases (in sequences 1d–e), the stratal geometries change: sediment deposition becomes localised in two areas: firstly in the most proximal setting, where an aggrading carbonate shelf margin forms, and secondly, 1.5 km seaward of the main shelf margin, where an isolated platform develops (see photograph A in Fig. 14). This platform is considered to be roughly circular in plan view (by comparison with other isolated platforms in the area where the topographic form is clear from maps) and is 500 m in diameter. Sediment production on this platform finally gives up as the retrogradation accelerates prior to the formation of the maximum flooding surface. The isolated platform is then buried in marls, while the platform continues to aggrade in the more proximal setting. The maximum flooding surface of sequence 1 is defined from both the geometries and the facies. It is defined in geometries by the most landward retreat of the large-scale clinoforms observed at the northern (proximal) end of the transect. It is defined in facies by an interval of marls (facies 12) blanketing the platform.

7.1.3. Highstand 1 (parasequences 1f and g)

During the highstand of sequence 1, the shelf margin progrades (parasequences 1f–g). The shelf and slope morphology is shown in Fig. 14 in photograph D. At the end of this sequence, a sea-level drop of over 100 m exposes the shelf-top (evidence for this sea-level fall is discussed in the description of Sequence 2 below). The steep shelf margin collapses, sending slump deposits 2 km out into the basin. The shelf-margin is prone to collapse because of slope-steepening during progradation, but it seems that the exposure event provided the necessary perturbation to provoke major slope collapse. Meteoric dissolution that started during shelf-margin exposure may have provided the necessary mechanical weakening of the shelf margin to initiate catastrophic slope failure.

7.2. Sequence 2

7.2.1. Sequence boundary 2

Sequence boundary 2 formed during the major sea-level drop at the end of sequence 1. This major sea-level fall has been identified principally from the stratal relationship observed between the highstand of sequence 1 (parasequences 1f–g) and the lowstand of sequence 2 (parasequence 2a). Parasequence 2a is a wedge of autochthonous coralgal framestones (facies 1) deposited in a shallow marine environment. It has planar well-bedded internal stratal geometries, and onlaps the irregular top of the slump deposits. These slumps sit at the toe-of-slope of the sequence 1 shelf-margin. This shelf-margin is estimated to have a vertical relief of approximately 100–150 m, measured from the height of the slope clinoforms. Thus, a sea-level fall equivalent to roughly this slope height (100–150 m) is inferred from this stratal relationship. On the shelf-top at the northern extremity of the Pirinç transect, the sequence boundary has not been observed in detail because it was inaccessible in outcrop. From field and photograph observations of the geometries, a conspicuous surface on the platform top is proposed as the approximate position for sequence boundary 2. At the foot of the shelf-slope where the sequence boundary is accessible, it has been

recognized as a karst-surface at the top of a shallowing-up facies trend (described in the proximal log of Fig. 13). Here, the sequence boundary is irregular, eroded, and has 50-cm karst pipes infilled with massive calcitic spar. Thin sections show extensive dissolution features beneath this surface. In a basinal position, sequence boundary 2 is placed on the top of the slump units. The slumps are interpreted to have formed during sea-level fall prior to the deposition of sequence 2 lowstand, and the slump top is a distinct onlap surface for sequence 2 lowstand deposits (parasequence 2a).

7.2.2. Lowstand 2 (parasequence 2a)

The lowstand of sequence 2 (parasequence 2a) develops as a 10 m-thick wedge of in situ coralgal framestones deposited in a shallow marine environment. It onlaps the underlying slump-deposits in an updip direction, and down-dip, it thins laterally into basinal marls (facies 12).

7.2.3. Transgression 2 (parasequence 2b)

During the transgression of sequence 2, sea level rapidly rises, reflooding the shelf slope and top that were exposed during lowstand times. However, no sediments belonging to the sequence 2 transgression have been identified in this area. This is probably because of the steep slope formed by the underlying shelf-margin of sequence 1, which does not provide a stable surface for accumulation of significant thicknesses of shallow-platform carbonate sediments. The position of the maximum flooding interval has been inferred from the stratigraphic reconstruction as occurring somewhere within the marls above the sequence 2 lowstand (and below the sequence 3 lowstand which has yet to be described).

7.2.4. Highstand 2 (parasequences 2c and d)

During the sequence 2 highstand, the shelf top is once again flooded and parasequences 2c–d (not distinguished from one another here) are deposited. These parasequences have not been logged in detail in the Pirinç area, as they are inaccessible. Their bedding geometries show parallel bedding on the platform top with some thickening at the shelf margin. Prograding geometries "backfill from the margin north into the internal platform, indicating that some shelf-margin topography formed at times. A large sea-level fall of 100–150 m marks the end of this sequence. The shelf-margin collapses sending slump deposits over a kilometer into the basin. These slump deposits are shown in photograph C in Fig. 14: this example is situated in a distal position in the basin (at the toe-of-slope) and consists of large (10 m or larger) boulders of shelf margin shallow marine carbonate sediments mixed with basinal marls. The mechanism and timing of slope collapse relative to sea-level fall is considered to be the same as for the end of sequence 1. Exposure of the shelf top and associated dissolution processes weakens the slope which is already at a critical angle. This results in catastrophic collapse of the slope sediments during sea-level fall.

7.3. Sequence 3

7.3.1. Sequence boundary 3

Sequence boundary 3 is defined in the same manner as sequence boundary 2. On the platform top, it is a major exposure surface, while in the basin, it is the top of the second slump packet described above (late highstand deposits of sequence 2). The position of this sequence boundary on the platform top is determined by identifying the highest bed truncated by the erosional scar of the sequence 2 slumping event. The sequence boundary on the platform top is inaccessible in the field but was observed at the top of the slump scar. Here, some evidence for exposure has been preserved: this consists of brecciated limestones in a ferruginous matrix and ferruginous, laminated sediment filling centimetre-sized cavities in the limestone. The top of the slumps in the basin is onlapped by parasequences 3a (sequence 3 lowstand) and 3b and c (sequence 3 transgression) in a basinal position. These parasequences are shallow-marine carbonate deposits. The juxtaposition of these shallow-marine deposits with underlying basinal sediments and slumps is the key evidence for major sea-level fall at this time. The amount of sea-level fall is estimated from the height of the slope that formed during sequence 2: this has been measured as 100–150 m.

7.3.2. Lowstand 3 (parasequence 3a)

Parasequence 3a forms the lowstand of sequence 3. It has a thin wedge geometry, thickening to 8 m maximum thickness, and thinning updip to an onlap-

ping pinch-out against the underlying topography formed by sequence boundary 3. Internal bedding geometries are planar and horizontal, with low-angle onlap at the base of the parasequence. Near to the top there is a series of iron-encrusted surfaces interpreted as hardgrounds formed during flooding. The top shows a progressive deepening into marls (facies 11). The facies of parasequence 3a are mostly clean coralgal framestones (facies 1). They contain in situ dome and plate-corals with a large amount of stick-coral debris. 30–60-cm bedding is defined by shaley partings. These shales are interpreted to have come from the Paleo-Goksu river, which was situated at the time to the northwest of the basin. Terrigenous material, normally not observed in the Pirinç section, was brought out this far by the lowstand conditions that prevailed at the time of deposition of parasequence 3a.

7.3.3. Transgression 3 (parasequences 3b and c)

Parasequences 3b and c are deposited during the transgression of sequence 3. They are deposited in progressively more updip locations compared to parasequence 3a, forming a backstepping trend. Parasequences 3b and c form wedges with a maximum thickness of 15–20 m. In an updip direction, they progressively onlap the underlying sequence boundary 3. Parasequence 3b is made up of dominantly coralgal framestones (facies 1) with some Miliolid grainstones (facies 10). Parasequence 3b is comprised dominantly of Miliolid grainstones (facies 10) near the updip onlap, changing basinwards to Nummulitid grain-packstones (facies 11) and eventually marls (facies 11) in the most basinward position. Parasequence 3b is shown in photograph B of Fig. 14. These marls are the highest sample that shows an NN4 biozone age.

7.3.4. Highstand 3 (parasequences 3d and e)

Parasequences 3d and e are deposited on the shelf-top and constitute sequence 3 highstand. This interval was not logged in detail on the shelf-top because it was inaccessible in the field, although its bedding geometries are described. These are dominantly planar on the shelf-top, although there are some progradations directly overlying sequence boundary 3. These "prograde north towards the platform interior, effectively "backfilling the shelf area. At the toe-of-slope, a wedge of sediment accumulates during highstand deposition. This wedge onlaps the slope in an updip direction and offlaps in a downdip direction. It is composed of very well bedded Nummulitid grain-packstones (facies 9) and has been interpreted as a toe of slope wedge, deposited as sediment from the shelf top, by-passes the steep slope, and accumulates in a lower slope position. The shelf edge is truncated by a steep erosional surface that is a slump scar. The slump deposits are observed at the toe-of-slope (overlying the toe-of-slope wedge). The timing of this slumping is uncertain. By analogy with the previous 2 slumps that occur during the late highstands of sequences 1 and 2 (triggered by sea-level fall), we can propose that a third sea-level fall may have occurred. However, as the sediments overlying this third slump have not been preserved in the outcrop, we cannot demonstrate this from the stratal relationships.

8. Depositional history of the Silifke transect

The Silifke study area is located in the south of the Mut Basin, northwest of the town of Silifke along a 20-km gorge trending northeast. Within this area, observations made at a number of key sites have been correlated to generate the cross-section presented in Fig. 6 (lower transect). The line-of-section cuts southwest to northeast: this direction is chosen inasmuch as it is approximately parallel to the structural dip of the basement graben feature that controls the Miocene depositional evolution. In the cross-section, the facies distribution has been simplified to distinguish between shallow water platform carbonates, basinal marls, slump deposits, basement, and Derinçay Formation continental conglomerates. During the Burdigalian, there is no major source of siliciclastic input in this area. Small local siliciclastic sources (minor streams) occur, but these are not distinguished in the cross-section shown in Fig. 6. In reconstructing this cross-section, the vertical thicknesses shown are controlled by logs and by relative altitude data from altimeter measurements and from map contours. The relative vertical position of each outcrop has been normalised to a datum: the top of parasequence 1e, which forms a distinct surface in the Silifke area. The full set of observations used to construct this cross-section is described in Bassant (1999). The Silifke Gorge during the Burdigalian forms an east–southeast-trending half-

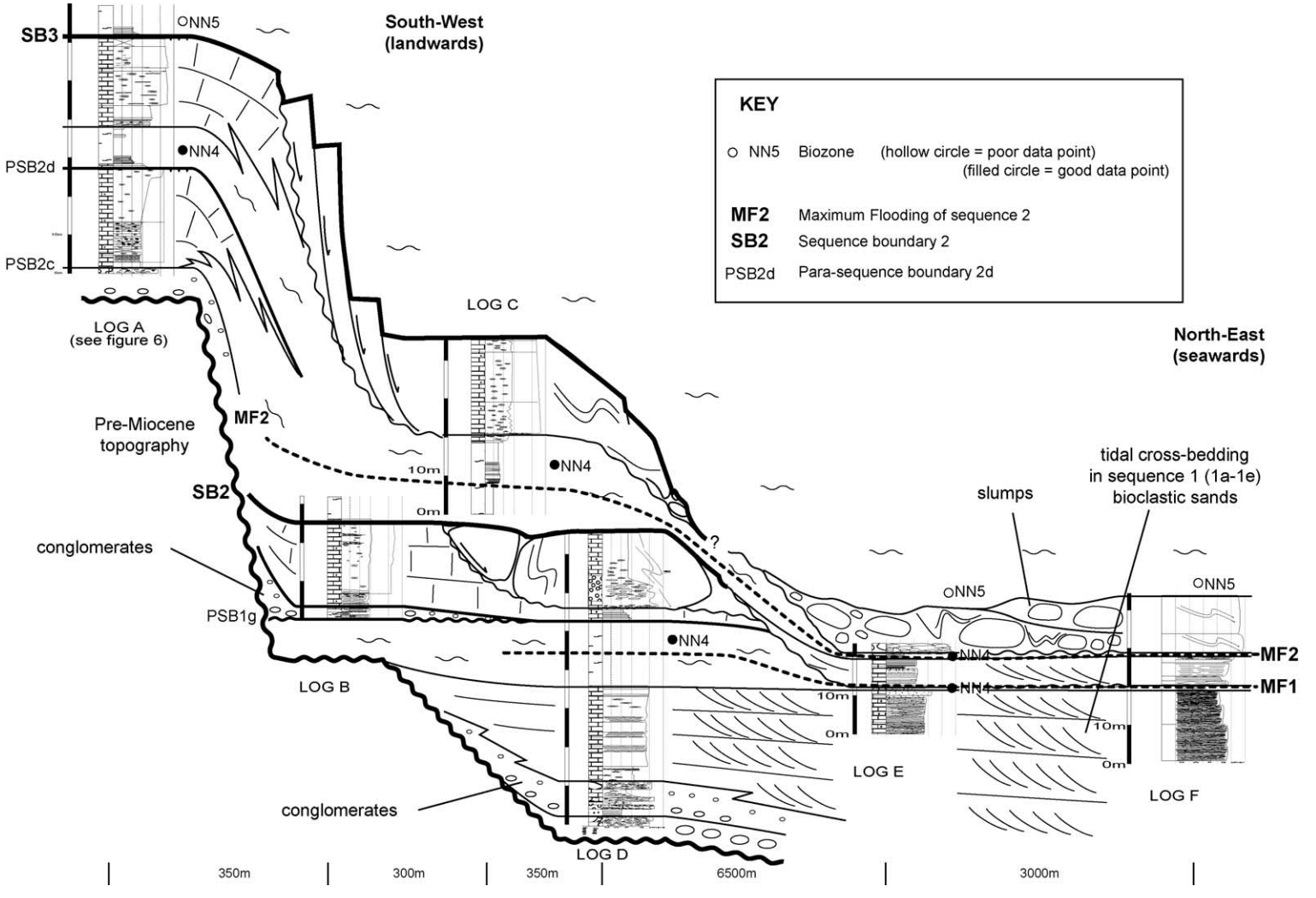

Fig. 15. Silifke logs. This shows the detailed correlations from the southern flank (Dibekli) to the centre of the strait.

graben. The major fault forms the steep, southern graben-wall, while the northern limit of the graben is the gently inclined tilted footwall-block sloping up to the north (Bassant, 1999). The sequence-by-sequence description that follows refers to both the summary cross-section in Fig. 6 and the detailed log correlation panel shown in Fig. 15. This figure illustrates the correlations between the southern flank of the graben (logs A–D) and the centre of the graben (logs E and F). Stratigraphic architectures from the southern flank and northern flanks of the graben are illustrated by the photographs in Fig. 16.

8.1. Sequence 1

8.1.1. Transgression 1 (parasequence 1a–e)

The transgressive deposits of sequence 1 (parasequences 1a–e) in this area are a tidal ramp system 3–7-km wide by 20–25-km long, infilling the strait formed by the Silifke graben. In the centre of the graben, they attain 80–100 m thickness, while on the flanks to the north and south, they onlap and pinch out against the graben walls. Lateral facies change occurs into marls in the deeper water areas at the eastern (Mediterranean) and western (Mut Basin) ends of the

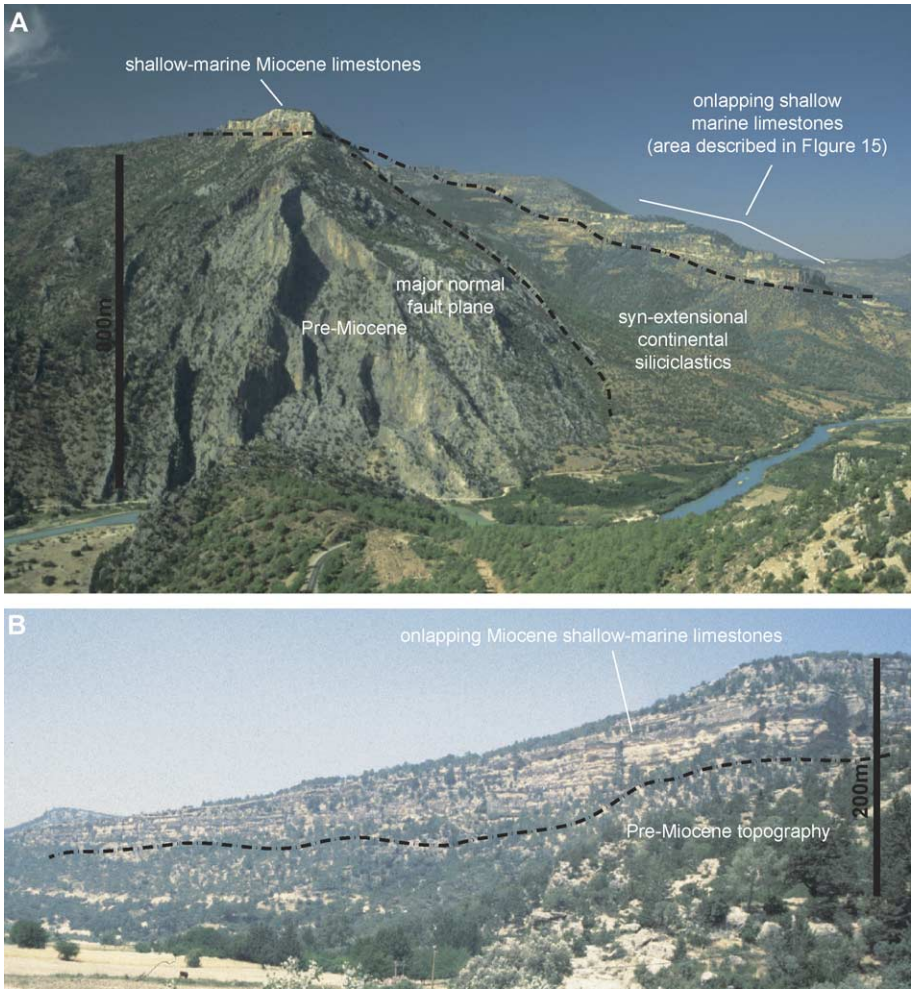

Fig. 16. Silifke photo 1: the Silifke graben margins. Photograph A shows the southern flank of the Silifke graben. The Pre-Miocene here forms a steep fault-controlled topography. Continental siliciclastics partially infill the space created during active faulting, and shallow-marine limestones then onlap the siliciclastics during marine flooding of the graben. The bottom photo B shows the northern flank of the Silifke graben, with shallow marine limestones of Burdigalian and Langhian age onlapping the Pre-Miocene, and the shelf-margin gradually backstepping.

strait area. The dominant facies type is the bryozoan grain-rudstone (facies 14). At the flanks of the strait, minor local streams input small volumes of sands and gravels. The limestone tidal deposits form cross-beds at a variety of scales, depending upon the local hydrodynamic conditions. Cross-bedding can be dominantly unidirectional, with rare bedding indicating a reverse flow. Most inferred current directions are close to the axis of the strait, and the flow direction commonly reverses over a short lateral distance between outcrops. It seems the ebb and flow currents were restricted to different channel systems, and these often remained static over the deposition of this lowstand packet. An outcrop of these sediments is illustrated in the lower photograph in Fig. 17. The rate of sea-level rise finally exceeds the rate of sedimentation during the flooding event at the top of parasequence 1e (which corresponds to the maximum flooding of sequence 1), and shallow-marine carbonate deposits in the centre of the strait are overlain by marls (facies 12).

8.1.2. Highstand 1 (parasequences 1f and g)

During sequence 1, highstand shallow marine carbonates are deposited against the northern flank of the graben (parasequences 1f and g). The facies are a mixture of detrital carbonate grainstones and rudstones (facies 9, 10, 11, and 13) and bioconstructed coralgal sediments (facies 1 and 5). Deposition on the southern flank of the graben during parasequence 1f is mostly planktonic foraminiferal marls (facies 12). A fringing platform is not observed to develop on this southern flank at this time: this may be due to the slope of the southern flank, which is too steep to provide a sufficiently wide habitat for the accumulation of carbon platform sediment. Additionally, some synsedimentary fault movement may be responsible for locally creating an increased accommodation rate and a steep actively fault-controlled flank. During the deposition of parasequence 1g against the northern flank of the graben, a fringing platform a few hundred metres in width develops. Facies are dominantly detrital carbonate sediments. During the deposition of parasequence 1g on the southern flank, coarse-grained fan deltas are observed to develop close to the basement onlap. These contain large metre-size boulders in places. Rapid lateral facies change occurs, and these fan delta deposits grade laterally over a distance of approximately 100 m basinwards into shallow marine carbonates. Aside from these fan deltas, siliciclastic sediment input at this shoreline is generally low. The main facies of the highstand on the southern flank are these shallow-marine carbonates. They are a variety of detrital and bioconstructed facies, with local small reefal developments (facies 1 and 5) surrounded by Miliolid and Soritid grainstones (facies 9 and 10). The seaward end of this margin has undergone gravitational collapse in many areas. This is notably observed in the southern flank area, which is detailed in the log correlations in Fig. 15. The incipient stages of slumping collapse can be observed in this area where well-cemented shallow marine limestones of the highstand have started to slide over the underlying marls of the transgression. Lateral displacement via slumping in this area is minor (a few metres) but increasing basinwards. Blocks are locally rotated and shunted, and the decollement surface beneath is irregular, scoured, and rucked. Some of the listric rotations indicate possible growth, telling us the slumping may have been contemporaneous with sedimentation. We propose that the mechanism for slumping in this area is by early differential compaction of the underlying transgressive marls, creating flexure in the brittle (due to early cementation) shallow-marine carbonates of the highstand, leading to gravitational creep and slumping.

8.2. Sequence 2

8.2.1. Lowstand 2 (parasequence 2a)

Sequence boundary 2 is placed at the top of the shallow-marine limestones of the sequence 1 highstand. Some large cavities in the underlying highstand may be due to exposure and karstification at this time, although the timing of this karst formation is not ascertained. A major relative sea-level fall is inferred by the relationship between the highstand of sequence 1 (parasequence 1f and g) and the lowstand of sequence 2 (parasequence 2a) from the mapped stratigraphic relationships and the stratigraphic reconstruction (Fig. 6). The precise value of the sea-level fall that occurred here is difficult to measure here due to postdepositional structural activity. The sequence 2 lowstand (parasequence 2a) is a 10-m packet of cross-bedded bryozoan grain-rudstones (facies 14) and rhodalgal grainstones with Nummulitid and Amphisteginid foraminifera

Fig. 17. Silifke photo 2: slump deposits and cross-bedded tidal deposits. The top photo shows a 20 m thick slump packet that sits at the NN4/NN5 biostratigraphic boundary (parasequence 2d). The lower photo shows a detail of the cross-bedded bioclastic grainstones and rudstones that fill in the base of the graben under the influence of strong tidal currents.

(facies 11), containing heterolithic sands in areas. These facies are very similar to those of the sequence 1 lowstand. This unit is deposited in the centre of the graben, stacked directly over lowstand 1. The two lowstands are separated by a maximum flooding surface of fine packstones (facies 11) to marls (facies 12). The sequence 2 transgression is very similar to that of sequence 1: on the northern flank of the graben, a backstepping, fringing platform develops, while on the steep southern flank, only planktonic foraminiferal marls (facies 12) are deposited. As in sequence 1, this lack of platform

development may be explained by the steepness of the antecedent topography further enhanced by synsedimentary faulting.

8.2.2. Transgression 2 (parasequence 2b)

The transgression of sequence 2 (parasequence 2b) is different on the northern and southern flank of the graben. On the gently sloping northern flank, it consists of a narrow fringing platform no more than a few hundred metres in width at most. The transgression onlaps the underlying Pre-Miocene topography (photograph B in Fig. 16). The platform margin at this time is dominantly retrogradational, and little to no slope sediments are preserved: a by-pass margin develops, and any sediments exported from the platform to the slope accumulate at the toe-of-slope. These sediments can be observed in a number of places around the Silifke Graben area and are distinguished form the lowstand deposits by their bedding morphology, as steeply dipping wedges accumulating locally against the toe-of-slope. They typically are planar-bedded with evidence for gravity flows and contain a mixture of platform- and basin-derived (planktonic) forams. The lowstand deposits of parasequence 2a do not typically contain planktonic forams and additionally contain some corals and encrusted with well-developed red-algal encrustations, indicating a relatively shallow environment of deposition. On the steeply dipping southern flank of the graben, no fringing platform develops, and only marls (facies 12) are deposited in direct onlap against the underlying Pre-Miocene topography. As in the transgression of sequence 1, the probable cause of this is the steepness of the slope, which does not provide a sufficiently wide shelf area for shallow marine carbonates to accumulate on.

8.2.3. Highstand 2 (parasequences 2c and d)

During the highstand on the northern flank, detrital carbonates are exported downslope from the platform top and deposited on the slope as distinct well-bedded gravity flows. These directly overlie the margin-edge of the backstepping transgression preserving the position of the transgressive platform margin. On the south flank of the graben, the highstand develops as a prograding carbonate platform. Here, the two parasequences 2c and d that form sequence 2 highstand can be clearly distinguished as two prograding packages separated by a flooding surface. Facies include Miliolid and Soritid grainstones (facies 10 and 9, respectively) and coralgal boundstones (facies 1). Red algae dominate as the main bioconstructor in this area. During this highstand, a plateau area formed by the antecedent topography on the southern flank was flooded, and the wide shallow-marine carbonate platform that was able to develop generated large amounts of detrital carbonates. This in turn led to rapid progradation of the platform edge. In areas where the platform prograded out over marls slumping, collapse is a commonly observed process. This can be seen in the log correlation panel shown in Fig. 15. It seems that the principle cause of slumping is the deposition of shallow-platform carbonates over soft compactable marls. Deformation of the marls due to loading may lead to catastrophic collapse of the overlying partially lithified shallow platform carbonates. This produces a mixture of brittle and plastic deformation slump structures. The top of the highstand on the southern flank is a major exposure surface. Microcodium is observed in thin-section just beneath the surface as well as large-scale dissolution features (pipes and cavities) and brecciation with ferruginous infill near the exposure surface. This brecciation may be associated with palaeosol formation close by. This exposure event may also have played a role in enhancing the slumping process in a similar fashion to that described for the Pirinç slumps. This exposure surface is also a significant biostratigraphic boundary. Marls found below have been dated as NN4 (Late Burdigalian to very Early Langhian), while marls above are the first occurrence of NN5 (Langhian) observed in the area. Redeposition during this slumping event carries slump material down into the centre of the graben. Here, it forms a semicontinuous unit of shallow marine carbonate blocks 10–20 m thick (see Fig. 15 and the upper photograph in Fig. 17). As on the graben flanks, this slump unit forms the boundary between NN4-age marls below and NN5-age marls above. Sequence 3 has not been described in this study because we focused on the NN4 interval.

9. Correlations

The first line of reasoning for correlating geographically separate areas is the biostratigraphic dating. In each of the areas studied the position of

the NN4/NN5 biozone boundary has been established with varying degrees of accuracy. The biostratigraphic dates (tops and bases of first occurrence) are shown on the cross-sections in Fig. 6. The uncertainty in attributing age to the stratigraphy has been captured by leaving a space for the possible position of the NN4/NN5 boundary between the highest NN4 and the lowest NN5 sample.

Alahan gives the best biostratigraphic control: here, the NN4/NN5 boundary is tied down to a 30-m interval above the base of parasequence 3e and below the sands that mark sequence boundary 4. In the distal position at the Kizil Kaya outcrop, all the samples analysed were NN4, except for one poor sample in the littoral muds beneath the build-up that indicated a possible NN3 age. This is the only such example found to date in the whole of the basin. So in Alahan, we can state that the NN4 biozone extends from the marine flooding of the continental siliciclastics of the Derincay Formation to the base of parasequence 3e. Thus, the NN4 biozone encompasses three third-order transgressions, including the initial marine flooding, and the boundary lies somewhere in the third highstand.

In the Pirinç area, the lowest sample was found in the distal marls of parasequence 1c just above the start of the marine flooding of the basin, while the highest NN4 sample was found in the distal marls of parasequence 3c. The lowest NN5 sample was identified in marls a few metre above the last NN4 sample, but its exact stratigraphic position is uncertain as the marl bed from which it was taken could not be followed readily updip. Its likely position is somewhere above the maximum flooding of cycle 3, and this uncertainty has been indicated in the age-column on Fig. 6. So in Pirinç, we can state that the NN4 biozone encompasses three third-order transgressions (including the initial marine flooding) and two major lowstands that juxtapose shallow marine carbonates during the lowstands against highstand deepwater (subphotic) deposits, and the boundary lies somewhere in the third transgression or highstand.

In the Silifke area, the lowest nannoplankton date established is NN4 from marly intervals within parasequence 1c. The highest NN4 sample in the southern graben flank area is from within parasequence 2d. The lowest NN5 sample is from the marls above sequence boundary 3 in log E and F (Fig. 15). In the basinal setting in log E (Fig. 15), marls below parasequence 3a are all NN4 in age, while marls above are NN5. The exact parasequence to which the first NN5 samples belongs to is uncertain, but sea level probably occupied a highstand position at the time of NN4/5 transition in order to deposit marls in the basinal and margin (Dibekli) setting. This is consistent with the position of the observed transition in Alahan where it occurs in the late transgression–highstand of sequence 3. So in Silifke, we can state that the NN4 biozone encompasses three third-order transgressions (including the initial marine flooding) and at least one, and possible a second, major forced regressions that juxtapose shallow marine carbonates during the lowstands against highstand deepwater (subphotic) deposits, and the boundary lies somewhere in the upper part of the third transgression.

Hence, three and only three third-order cycles (three relative sea-level rises, and two falls) can be identified in each of the study areas between the time of initial marine flooding and the NN4/5 biozone boundary, and this biostratigraphic boundary occupies the late transgression to highstand times of the third relative sea-level rise. This permits the three sequences (1–3) to be correlated across the Mut Basin with reasonable certainty.

Once this sequence framework is established, we need to correlate at the parasequence scale. Generally, the biostratigraphy does not provide a guide for this level of correlation. Only in the Alahan–Kizil Kaya transect does it constrain the NN4/NN5 boundary to within the resolution of a parasequence. Thus, in order to correlate parasequences within a sequence across the basin, we need to apply an alternative technique to biostratigraphy. To do this, we construct then correlate the relative sea-level curves for each transect, allowing us to propose correlations at the scale of parasequences across the basin. The methodology is described below.

10. Discussion

10.1. Estimating sea-level change

Relative sea-level changes have been calculated for each of the transects. The process used to calculate these is similar to the pinning-point methodology of

Goldstein and Franseen (1995). In order to minimize the effect of postdepositional tilting and flexing, the relative sea-level curve was calculated on a vertical section where possible (e.g., Alahan, Zincir Kaya). However, where facies belts shift laterally between highstands and lowstands (e.g., in Pirinç), postdepositional flexure and tilting were estimated and removed from the calculated value for relative sea-level change. A significant example of this is the measurement of the relative sea-level change between highstand and lowstand conditions in the Pirinç cross-section. Here the height of the clinoform margin was used; this was reasonably well constrained, having been physically measured using detailed mapping, logging, and repeated altimeter measurements. No attempt was made to remove the effects of compaction from the calculation. Fig. 18 shows the results of these calculations. The vertical axis is the relative sea-level value in metres. The horizontal axis is an arbitrary time axis, with time advancing to the right. The time

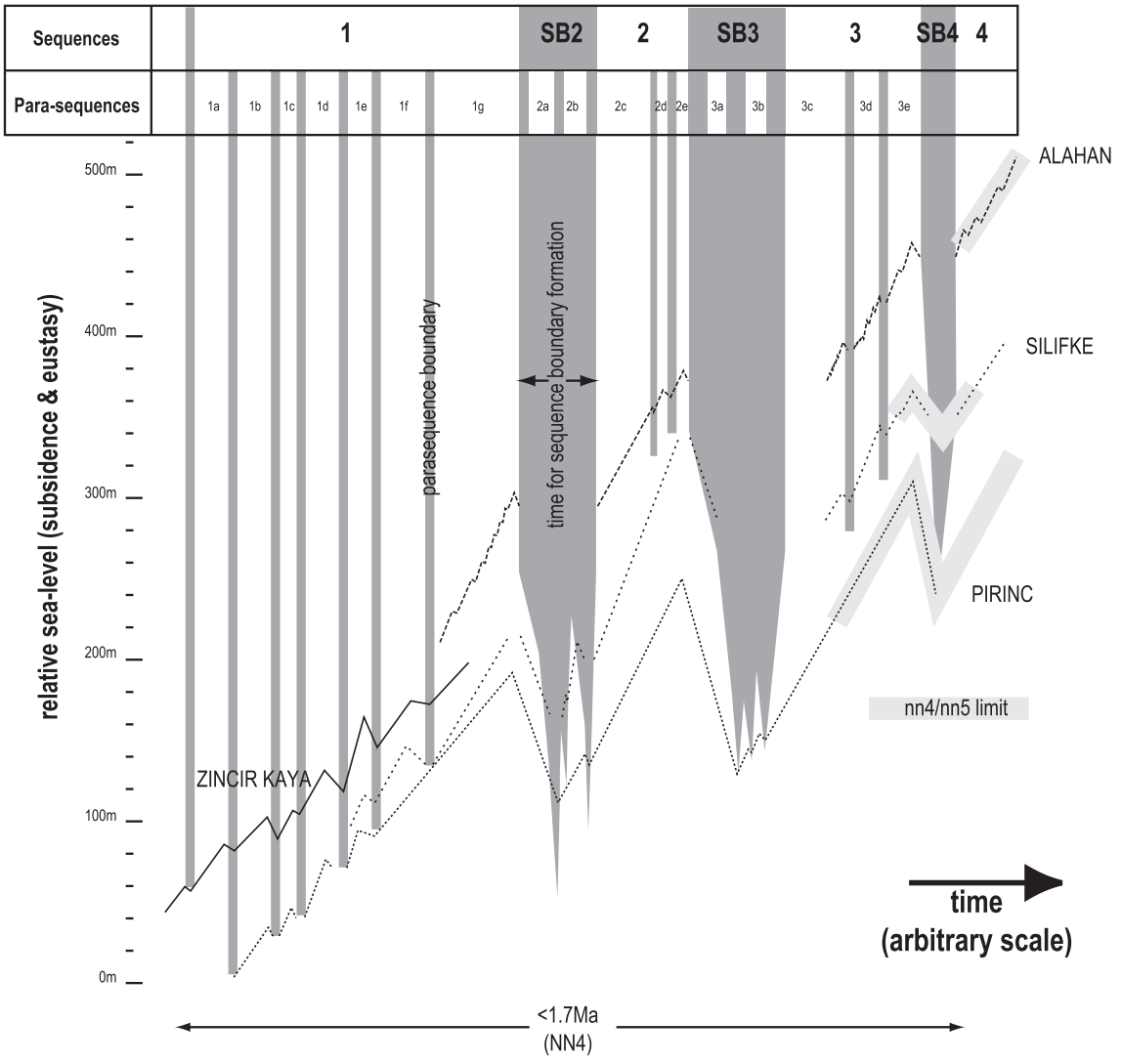

Fig. 18. Relative sea-level curves. These are the relative sea-level curves for the three study sites: Alahan, Pirinç, and Silifke. Zincir Kaya is an isolated platform close to the Alahan cross-section. The horizontal axis is arbitrary time, while the vertical axis is relative sea level (eustasy plus subsidence). The temporal positions and hierarchy of sequence and parasequence boundaries are indicated.

interval examined is the NN4 biozone (Late Burdigalian to Earliest Langhian), which is approximately 1.7 Ma in duration (Martini and Müller, 1986). This is a maximum value for the interval studied, as the base of the NN4 biozone has not been defined in most areas. Sequences and parasequences are defined at the top, with the vertical thick grey lines indicating the time allotted to sequence boundary formation and the thin vertical grey bars showing the flooding surfaces that define the parasequences. The relative sea-level curves generated from the different areas have been spaced vertically for the purposes of presentation; their vertical position is not significant, what is important is the shape of each curve. Each curve captures different time intervals of the relative sea-level signal, depending on the stratigraphic position of the outcrop. For instance, in the Alahan section of the Alahan–Kizil Kaya transect, only the transgressions and highstands are preserved, and we have no record of how far relative sea-level falls during the lowstands. In Kizil Kaya, we see only the sequence 1 transgression; however, this record is preserved in good detail. In the Pirinç cross-section, we have the best control because we observe both the highstands and the lowstands. Theoretically, a relative sea-level curve is specific to one point on the Earth's surface. We can calculate a relative sea-level curve for a cross-section only by assuming that there is no significant differential subsidence along the length of the cross-section within the study time interval. Bearing this in mind, it is striking that the relative sea-level curves calculated from different areas across the basin area are so similar. It is tempting to propose a single relative sea-level curve for the whole basin (though we have not done that here). The part of the signal that may change significantly across a basin is the subsidence rate (the eustatic signal will be same everywhere). This may be due to the fact that little significant synsedimentary faulting is observed in the NN4 time interval in the areas studied apart from the Silifke area. Even in the Silifke area, it is significant only because of its role in controlling the development of carbonate platforms by forming topography and because seismic activity associated with small fault movements may have helped to provoke slumping. The variations in accommodation (throws on the faults) during this period due to faulting are on the order of 10 m or less, and this is not too significant when we have relative sea-level variations of 100–150 m occurring. Subsidence occurs during this time, but it seems as if the dominant tectonic process is basin-wide (epeiric) subsidence, with the whole basin subsiding as one single entity.

These relative sea-level correlations allow us also to correlate parasequences between the three different transects in the basin. These parasequence-scale correlations are shown as a Wheeler diagram (chronostratigraphic representation) in Fig. 19. These correlations allow us to compare contemporaneous sedimentary environments across the basin, and the implications of this are discussed below.

10.2. Causes of sea-level change

The two scales of stratigraphic cycles considered here (sequences and parasequences) correspond to two distinct scales of relative sea-level cyclicity (see Fig. 18). The sea-level variations associated with sequence-formation are cyclical rises and falls of around 100–150-m amplitude. Three rises and two (possibly three) falls occur in less than 1.7 Ma. If we simply divide the total time by the number of sequences within this time-interval, the average duration of these relative sea-level cycles is 570 Ka or less. These may correspond to the 400-Ka Milankovitch eccentricity cycles. The sea-level cycles associated with the formation of the parasequences have an amplitude of around 18–30 m. Sixteen of these cycles occur in a time interval of less than 1.7 Ma, thus the average duration of these parasequences is 106 Ka or less. These may correspond to the 100-Ka Milankovitch obliquity cycles. We consider that these relative sea-level cycles are probably caused by eustasy. It is difficult to imagine a structural mechanism that would uplift and subside the entire Mut Basin with such cyclic regularity on a 100 and 570 Ka timescale. Other evidence (faulting and deformation) would be visible within the basin if such a tectonic regime was active, and this is not seen. On the other hand, in the Late Burdigalian, the East Antarctic ice sheet was already formed, and the West Antarctic ice sheet was in the process of formation (Abreu and Anderson, 1998). Thus, sufficient ice volume was stored in Antarctica to drive significant glacioeustasy. Because the West Antarctic ice sheet was in the process of forming, it may have been exceptionally sensitive to climatic variations. Glacioeustatic sea-level variations

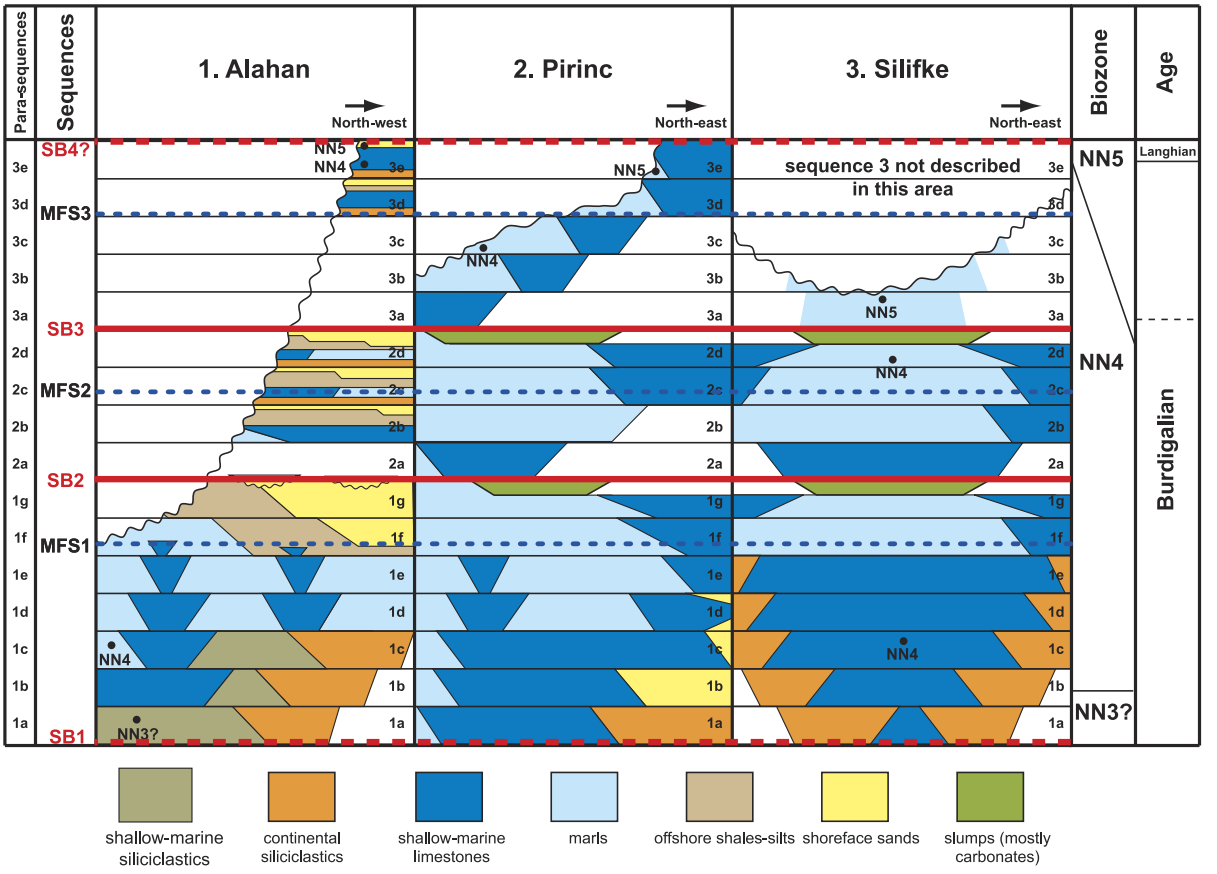

Fig. 19. Mut Basin chronostratigraphic summary. The temporal relationships between the different stratigraphic units in the transects are shown in this Wheeler diagram. The vertical axis is approximately time. In sequence 1, we see how the tidal deposits of Silifke are synchronous with the isolated platforms of the Mut area.

are often most sensitive to the long- and short-term Milankovitch eccentricity cycles of 400 and 100 Ka (Read et al., 1995), and this is consistent with the duration of the cycles observed (described above). Oxygen isotope data (Abreu and Anderson, 1998) are consistent with high-amplitude glacioeustatic cycles during the Late Burdigalian and Langhian. Lowstands of sequences 2 and 3 (NN4 Nannoplankton biozone) in this study may correlate to the MBi-3 and MLi-1 oxygen isotope events (positive peaks in the O-18 signal), while the lowstand of sequence 3 (if it exists) may correlate to the MSi-1 peak. Additionally, the eustatic sea-level curve of Haq et al. (1987) features two major sea-level lowstand deviations of a magnitude of around 100 m at the base and top of the Langhian, which correspond approximately to the MLi-1 and MSi-1 excursions. This suggests that stratigraphic evidence for large (100 m) sea-level cycles occurs in other basins around this time, although the exact correlation to the Haq et al. (1987) curve is uncertain.

10.3. Impact of antecedent topography and relative sea-level change on depositional environments

The parasequence-scale chronostratigraphic correlations summarised in Fig. 19 permit us to compare contemporaneous sedimentary environments across the basin and understand how they evolve through time. Doing this, we see significant variability of depositional settings across the basin: these differences can be explained in part by the complex basin morphology (antecedent topography) and the interaction between this and the high-amplitude sea-level

1. Sequence 1
transgression
(para-sequences 1a-e)

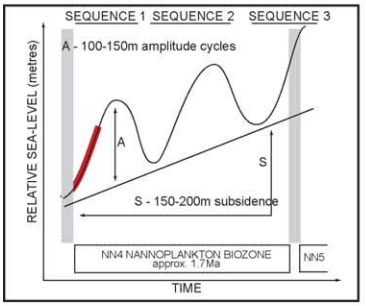

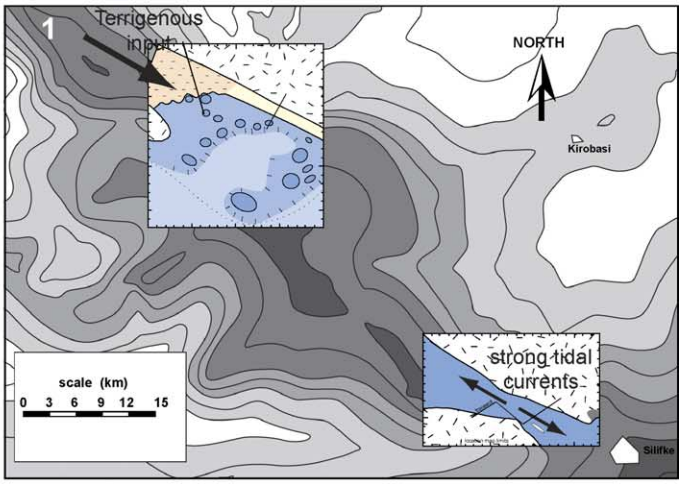

2. Sequence 1
highstand (para-sequences 1f-g)

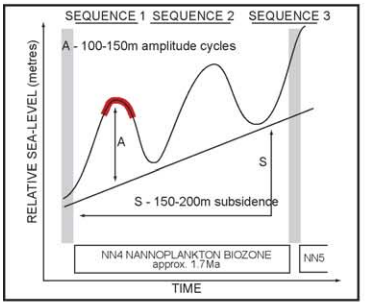

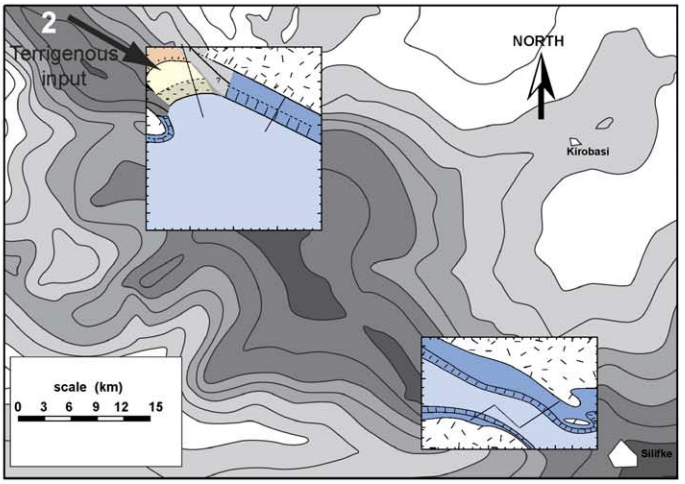

3. Sequence 2
lowstand (para-sequence 2a)

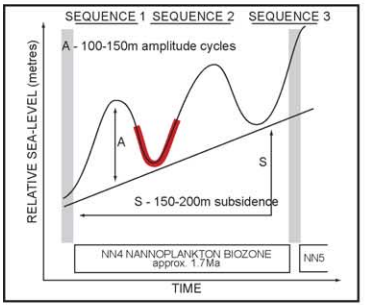

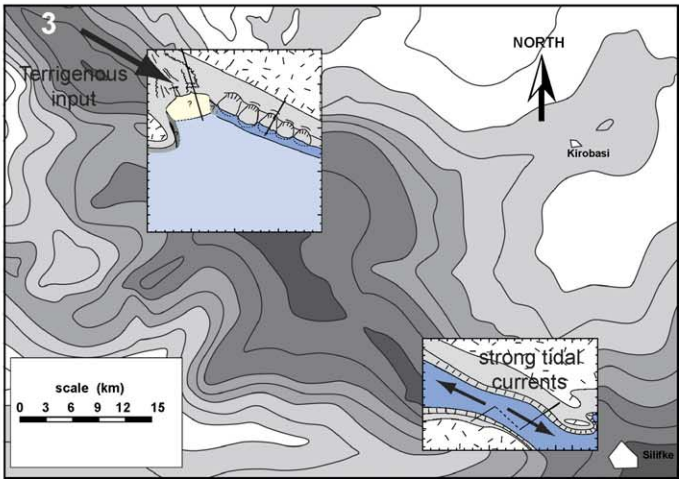

changes. The antecedent topography formed by the underlying Pre-Miocene syn- and preextensional rocks has a dramatic influence on the distribution of depositional environments across the basin. Apart from the direct control on the position of the coastline, and the slope of the sea floor, it also indirectly controls the distribution of current and wave energy. The combination of high-amplitude sea-level cycles and complex palaeotopography generates a complex depositional-environment distribution. In Fig. 20, the depositional environments across the basin are reconstructed for different time intervals. Cartoon 1 at the top shows the initial transgression of sequence 1. Cartoon 2 shows the sequence 1 highstand, and cartoon 3 reconstructs the lowstand for sequence 2. During transgression 1, the Silifke strait area (formed as a graben) acts as a funnel focusing strong tidal currents, producing the coarse cross-bedded carbonate tidal deposits. Some locally sourced heterolithic siliciclastics are present in this interval but are volumetrically insignificant. The hinterland drainage system brings terrigenous material only into the northwestern corner of the Basin. This drainage pattern is directly controlled by the northwest-striking fault trend that dominates in this area; the grabens serving as conduits to focus sediment flow. In the northwest corner of the Basin away from the influence of the strong tidal currents found in the Silifke strait, the isolated platform complex develops. The locus of distribution of these platforms seems to be tightly controlled by the form of the underlying delta (Eriş et al., 2004). When this delta was flooded and siliciclastic deposition was pushed back, the delta top formed a wide shallow-water gently sloping surface. This morphology was ideal for the development of a carbonate platform (except for the input of siliciclastics at the coast to the northwest). The transition from a marine siliciclastic to a carbonate environment can be seen at the base of the platforms. The largest isolated platforms are around the seaward edge of the delta top (highest energy conditions and furthest from the siliciclastic source), with platform growth stopping abruptly at this edge. The position of isolated platforms also seems to be controlled by the underlying fault-block morphology generated during the basin formation. Although this morphology is mostly buried by thick layers of sediment, it still subtly influences the sea floor topography because of differential compaction over these blocks. During sequence 1 highstand times, the relative sea-level rise of 180 m (this includes eustasy and subsidence, and is taken from the Pirinç sea-level curve in Fig. 18) over the basin topography dramatically changes the hydrodynamic parameters in the Basin. The Silifke strait area is wider and deeper, and strong tidal currents are no longer a controlling factor in facies development in Silifke. Narrow fringing platforms (bioconstructed and detrital carbonate sediments) develop on the graben flanks but only in areas where the underlying topography is not too steep. Because the graben is asymmetric, with a steep fault on the south, the fringing platform is wider on the northern flank and often not present on the south. In the north of the basin (Fig. 20), the relative sea-level rise has flooded and drowned the isolated platforms that developed during lowstand transgression, the shoreline has migrated north, and the sea-floor drops away rapidly to subphotic depths (150 m+). So in this area too, a narrow fringing platform develops. In the northwest corner (Alahan transect), the siliciclastics prograde and form a sandy shoreline. During lowstand 2 (cartoon 3 in Fig. 20), relative sea level lowers dramatically again (by about 80 m from the Pirinç relative sea-level curve in Fig. 18), and the Silifke strait once again becomes a narrow passage with strong tidal currents developing. In the northern part of the basin around the Pirinç transect, narrow lowstand carbonate wedges develop over the isolated platforms. The siliciclastic response is not preserved in outcrop.

Fig. 20. Palaeogeographic maps of the Mut Basin. This reconstructs the depositional environments across the Mut Basin for (1) the sequence 1 transgression, (2) the sequence 1 highstand, and (3) sequence 2 lowstand. Two high-amplitude (100–150 m) relative sea-level cycles occur within the study time interval in the Mut Basin, and these have a dramatic impact on the palaeoenvironmental distribution. (1) During the initial marine flooding (NN4 biozone, Late Burdigalian–Early Langhian), an isolated platform complex develops across a shallow shelf area in the north of the Mut Basin, while in the south, a high-energy tidal ramp system develops within the straits that connect the Mut Basin to the Mediterranean Basin. (2) During the highstand of sequence 1 (NN4), fringing platforms develop around the basin margin onlapping the antecedent basin topography. (3) During the sequences 2 lowstand, slumping of the highstand platform occurs, and lowstand shallow-marine carbonates onlap the distal ends of the slump packets in the north of the Mut Basin. In the south in the Silifke Graben, the tidal ramp system once again develops. This diagram uses the same facies colours as the transect panels (Fig. 7).

11. Conclusion

Stratigraphic reconstructions from the Mut Basin show two orders of relative sea-level cycles occurring in the NN4 biozone interval studied (the Late Burdigalian to Early Langhian). These have been interpreted to be eustatic cycles. The large-scale eustatic cyclicity (producing sequences in the stratigraphic record) has an amplitude of around 100–150 m and may be driven by the long-term 400-Ka eccentricity orbital cycle. Two, and possibly three, lowstand units have been identified as being produced by this scale of cyclicity, and they can be correlated with the oxygen isotope curve published by Abreu and Anderson (1998) and to some degree with the Haq curve (Haq et al., 1987). The short-term eustatic cyclicity (producing parasequences in the rock record) has an amplitude of 18–30 m and may be driven by the 100-Ka short-term eccentricity orbital signal.

Glacial eustasy, with melting and forming of the Antarctic icecap, is proposed as the main mechanism for driving eustasy in these cycles. Identification of this eustatic signal is important because it is a documented example of a rapid (400 Ka) high-amplitude (100–150 m) eustatic sea-level change that occurs outside of the Holocene. Also, many of the recent deepwater oil discoveries (Gulf of Mexico, USA, and offshore West Africa) are in early Miocene deep marine fans, with the timing of sand input possibly closely controlled by high-amplitude eustatic sea-level variation.

The stratigraphic reconstruction made in this study illustrates how high-amplitude sea-level cycles and steep complex antecedent topography combine to produce highly complex geographic distributions of depositional systems that can vary rapidly in nature through time. For lithostratigraphic predictions to be successful in such an environment (icehouse climate, early postrift tectonic setting with remnant topography due to incomplete erosion of hinterland and underfilled basins), we need to consider the interaction between relative sea level and topography.

Additionally, while many excellent examples of late Miocene carbonate platforms exist across the Mediterranean region and throughout the world, early Miocene carbonate outcrops are rare. The excellent outcrop quality and diversity of stratigraphic architectures thus make the Mut Basin an ideal reference model for Tethyan Burdigalian carbonate and mixed systems, with applications to petroleum reservoirs in Iran and Iraq and in the Far East (Bassant et al., 2004).

Acknowledgements

The authors would like to express their thanks to the Institut Français du Pétrole (IFP), Total and Elf (now Total), and the Swiss National Research Fund who financed this study. Also, many thanks to Kadir Eriş and Gursel Sinan (Istanbul Technical University), and to Christophe Prince (Open University, UK) for their help in the field. Thanks also to all the earth scientists at the IFP, Total, Elf, and the University of Fribourg who were generous with their time and suggestions. We would specifically like to acknowledge the support and advice of Robert Boichard, Philippe Lapointe, Herbet Eichenseer, and Peter Homewood. Many thanks to Werner Piller (University of Graz, Austria) for teaching us much about early Miocene fauna and flora, and thanks also to Jürgen Schlaf, Mathias Harzhauser, and Oleg Mandic for productive and fun collaboration in the field and guidance on all things to do with molluscs. Biostratigraphic analysis was fundamental to this project, and we warmly thank Carla Müller (IFP) for performing the Nannoplankton analyses, and Roland Wernli (University of Geneva) for performing the foraminiferal biostratigraphic analyses.

References

Abreu, V.S., Anderson, J.B., 1998. Glacial eustasy during the Cenozoic: sequence stratigraphic implications. AAPG Bull. 82, 1385–1400.

Barron, J.A., Keller, G., 1982. Widespread deep-sea Miocene hiatuses: coincidence with periods of global cooling. Geology 10, 577–581.

Bassant, P., 1999. The high-resolution stratigraphic architecture and evolution of the Burdigalian carbonate-siliciclastic sedimentary systems of the Mut Basin, Turkey. PhD thesis. GeoFocus 3. University of Fribourg, 277 pp.

Bassant, P., Van Buchem, F.S.P., Strasser, A., Lomando, A.J., 2004. A comparison of two early Miocene carbonate margins: the Zhujiang carbonate platform (subsurface, South China) and the Pirinç platform (outcrop, Southern Turkey). In: Grammer, M., Harris, P.M. (Eds.), Integration of Outcrop and Modern Analogs in Reservoir Modeling, AAPG Mem., vol. 80, pp. 153–170.

Bizon, G., Biju-Duval, B., Letouzey, J., Monod, O., Poisson, A., Özer, B., Öztümer, E., 1974. Nouvelles précisions stratigraphi-

ques concernant les bassins Tertiares du Sud de la Turquie (Antalya, Mut, Adana). Rev. Inst. Fr. Pét. 29 (3), 305–325.

Bolli, H.M., Saunders, J.B., Perch-Nielsen, K., 1985. Plankton Stratigraphy. Cambridge University Press. 327 pp.

Broucke, O., Boichard, R., Van Buchem, F.S.P., 1998. Modélisation stratigraphic et étude de terrain d'un haut-fond carbonaté (secteur Ermenek, Bassin de Mut Turquie). Rapport Interne Total II.

Cavelier, C., Butterlin, J., Clermonte, J., Colchen, M., Guennoc, P., Guiraud, R., Lorenz, C., Ricou, L.-C., 1993. Late Burdigalian (18–16.5 Ma). In: Dercourt, J., Ricou, L.P., Vrielynck, B. (Eds.), Atlas Tethys Palaeoenvironmental Maps, Beicip-Franlab.

Dercourt, J., Ricou, L.P., Vrielynck, B. (Eds.), 1993. Atlas Tethys Palaeoenvironmental Maps, Beicip-Franlab, Paris.

Dercourt, J., Ricou, L.P., Kazmin, V.G., Le Pichon, X., Knipper, A.L., Grandjacquet, C., Sbortshhikov, I.M., Geyssant, J., Lepvrier, C., Perchersky, D.H., Boulin, J., Sibuet, J.-C., Savostin, L.A., Sorokhtin, O., Westphal, M., Bazhrnov, M.L., Lauer, J.-P., Biju-Duval, B., 1986. Geological evolution of the Tethys belt from the Atlantic to the Pamirs since the Lias. Tectonophysics 123, 241–315.

Dewey, J.F., Hempton, M.R., Kidd, W.S.F., Saroglu, F., Sengor, A.M.C., 1986. Shortening of continental lithosphere: the neotectonics of Eastern Anatolia—a young collision zone. In: Coward, M.P., Ries, M.C. (Eds.), Collision Tectonics, Geological Society, London, Special Publication, vol. 19, pp. 3–36.

Dunham, R.J., 1962. Classification of carbonate rocks according to depositional texture. In: Ham, W.E. (Ed.), Classification of Carbonate Rocks, AAPG Mem., vol. 1, pp. 108–121.

Eaton, S., Robertson, A.H.F., 1993. The Miocene Pakhna formation, southern Cyprus and its relation to the Neogene tectonic evolution of the Eastern Mediterranean. Sediment. Geol. 86, 273–296.

Embry, A.F., Klovan, J.E., 1971. A Late Devonian reef tract on northeastern Banks Island, Northwest Territories. Bull. Can. Petrol. Geol. 19, 730–781.

Eriş, K.K., Bassant, P., Ülgen, U.B., 2004. Tectono-Stratigraphic Evolution of an early Miocene Incised Valley-Fill (Derinçay Formation) in the Mut Basin, Southern Turkey. This volume.

Esteban, M., 1996. An overview of Miocene reefs from Mediterranean areas: general trends and facies models. In: Franseen, E.K., Esteban, M., Rouchy, J.-M. (Eds.), Models for Carbonate Stratigraphy from Miocene Reef Complexes of Mediterranean Regions, SEPM, Concepts in Sedimentology and Palaeontology, vol. 5, pp. 3–53.

Gedik, A., Birgili, S., Yilmaz, H., Yoldas, R., 1979. Geology of the Mut-Ermenek-Silifke (Konya, Mersin) area and petroleum possibilities. B. Geol. Soc. Turkey 22, 7–26.

Gökten, E., 1976. Basement rock units and the Miocene stratigraphy of Silifke region. B. Geol. Soc. Turkey 19, 117–126.

Goldstein, R.H., Franseen, E.K., 1995. Pinning points: a method providing quantitative constraints on relative sealevel history. Sediment. Geol. 95, 1–10.

Görür, N., 1994. Tectonic control in the development of a lower Miocene reef at a complex triple junction: depositional history of the Karaisali Formation of the Adana Basin, Turkey. Géol. Méditerr., 49–67.

Görür, N., Okay, F.Y., Seymen, I., Sengör, C., 1984. Palaeotectonic evolution of the Tuzgolu basin complex: sedimentary record of a Neotethyan closure. In: Dixon, J.E., Robertson, A.H.F. (Eds.), The Geological Evolution of the Eastern Mediterranean, Geological Society, London, Special Publications, vol. 1 (7), pp. 467–482.

Gürbüz, K., Uçar, L., 1995. Book view Miocene biohermal reef bodies in the Mut Basin, Southern Turkey (abstract). Second International Turkish Geology Workshop 1995. Cumhuriyet University, Sivas, Turkey. Abstracts Volume.

Haq, B.U., Hardenbol, J., Vail, P.R., 1987. Chronology of fluctuating sea-levels since the Triassic. Science 235, 1156–1167.

Hsü, K.J., Cita, M.B., Ryan, W.B.F., 1973. The origin of the Mediterranean evaporites. International Report Deep Sea Drilling Project, vol. 13. United States Government Printing, Washington D.C, pp. 1203–1231.

James, N.P., 1984. Reefs. In: Walker, R.G. (Ed.), Facies Models, Geoscience Canada, pp. 229–244.

Janson, X., 1997. Etude des géométries et de la stratigraphie séquentielle haute résolution de la plate-forme carbonatée du bassin de Mut, dans la région d'Ermenek. Rapport de D.E.A. IFP, Paris.

Janson, X., Eberli, G., 2000. 2D/3D geometries of Tertiary prograding margins, Mut Basin, Turkey: interplay between accommodation and production Abstract. AAPG Bull. 84 (13).

Kelling, G., Gökcen, N.S., Safak, U., 1995a. Factors influencing genesis and evolution of Neogene Basins, Southern Turkey (abstract). Second International Symposium on the Geology of the Eastern Mediterranean Region, 1995, Program and Abstracts. Jerusalem, Israel.

Kelling, G., Safak, U., Gokcen, N.S., 1995b. Mid-Cenozoic evolution of the Mut Basin, South Turkey, and its regional significance (abstract). International Earth Sciences Colloquium on the Aegean Region 1995, Program and Astracts, Izmir, Turkey.

Korkmaz, S., Gedik, A., 1990. Study of source rock facies and petroleum occurrence in Mut-Ermenek-Silifke (Konya–Mersin) Basin, through geochemical methods. B. Geol. Soc. Turkey 33, 29–38.

Lauer, J.P., 1984. Geodynamic evolution of Turkey and Cyprus based on paleomagnetic data. In: Dixon, J.E., Robertson, A.H.F. (Eds.), The Geological Evolution of the Eastern Mediterranean, Geological Society, London, Special Publications, vol. 17, pp. 483–492.

Martini, E., Müller, C., 1986. Current Tertiary and Quaternary calcareous nannoplankton stratigraphy and correlations. Newslet. Stratigr. 16, 99–112.

Pierre, A., 2002. Modélisation numerique du système mixte silicoclastique/carbonate du Bassin de Mut (Burdigalien–Langhien, Turquie). Rapport de D.E.A. IFP, Paris.

Read, J.F., Kerans, C., Weber, L.J., Sarg, J.F., Wright, F.M., 1995. Milankovitch sea-level changes, cycles, and reservoirs on carbonate platforms in greenhouse and ice-house worlds. SEPM Short Course Notes 35.

Robertson, A.H.F., 1998. Mesozoic–Tertiary tectonic evolution of the easternmost Mediterranean area: integration of marine and land evidence. In: Robertson, A.H.F., Emeis, K.-C., Richter, C.,

Baroz, F. Proceedings of the Ocean Drilling Program, Scientific Results, vol 160, pp. 723–782.

Robertson, A.H.F., Dixon, J.E., 1984. Introduction: aspects of the geological evolution of the Eastern Mediterranean. In: Dixon, J.E., Robertson, A.H.F. (Eds.), The Geological Evolution of the Eastern Mediterranean, Geological Society, London, Special Publications, vol. 1 (7), pp. 1–74.

Robertson, A.H.F., Dixon, J.E., Brown, S., Collins, S., Pickett, E., Sharp, I., Ustaömer, T., 1996. Alternative tectonic models for the Late Palaeozoic–Early Tertiary development of Tethys in the Eastern Mediterranean region. In: Morris, A., Tarling, D.H. (Eds.), Palaeomagnetism and Tectonics of the Mediterranean Region, Geological Society, London, Special Publications, vol. 105, pp. 239–263.

Savostin, L.A., Sibuet, J.-C., Zonenshain, L.P., Le Pichon, X., Roulet, M.-J., 1986. Kinematic evolution of the Tethys belt from the Atlantic Ocean to the Pamirs since the Triassic. Tectonophysics 123, 1–35.

Schlaf, J., Mandic, O., Piller, W., Harzhauser, M., Bassant, P., 1997. Palaeoecology in the Lower Miocene of the Mut Basin (S. Turkey): European Palaeontological Society Meeting, Vienna, abstract.

Schlanger, S.O., 1981. Shallow-water limestones in oceanic basins as tectonic and paleoceaonographic indicators. In: Warme, J.E., Douglas, R.G., Winterer, E.L. (Eds.), The Deep Sea Drilling Project, a Decade of Progress, SEPM, Spec. Pub., vol. 32, pp. 209–226.

Schmidt, G.C., 1961. Stratigraphic nomenclature for the Adana region petroleum district VII. Petrol. Admin. Bull. 6, 47–63.

Sengör, A.M.C, Yilmaz, Y., Süngürlu, O., 1984. Tectonics of the Mediterranean Cimmerides: nature and evolution of the western termination of Palaeo-Tethys. In: Dixon, J.E., Robertson, A.H.F. (Eds.), The Geological Evolution of the Eastern Mediterranean, Geological Society, London, Special Publications, vol. 17, pp. 77–112.

Sengör, A.M.C., Görür, N., Saroglu, F., 1985. Strike-slip faulting and basin related formation in zones of tectonic escape. SEPM, Spec. Pub., 37, 227–440.

Sezer, S., 1970. The Miocene stratigraphy of the Mut Region. PhD thesis. Birbeck College, London University, 155 pp.

Steininger, F.F., Rögl, F., 1984. Paleogeography and palinspastic reconstruction of the Neogene of the Mediterranean and Paratethys. In: Dixon, J.E., Robertson, A.H.F. (Eds.), The Geological Evolution of the Eastern Mediterranean, Geological Society, London, Special Publications, vol. 1, 7, pp. 659–668.

Tanar, U., Gökçen, N., 1990. Mut-Ermenek Tersiyer istifinin stratigrafisi ve mikropaleontolojisi. MTA Dergisi 110, 175–180.

Westphal, M., Bazenhenow, M.L., Lauer, J.P., Pechersky, M.D., Sibuet, J.C., 1986. Paleomagnetic implications on the evolution of the Tethys Belt from the Atlantic Ocean to the Pamirs since the Triassic. Tectonophysics 123, 37–86.

Williams, G.D., Ünlügenç, U.C., Kelling, G., Demirkol, C., 1995. Tectonic controls on the stratigraphic evolution of the Adana Basin, Turkey. J. Geol. Soc. (Lond.) 152, 873–882.

Yetiş, C., 1988. Reorganisation of the Tertiary Stratigraphy in the Adana Basin, Southern Turkey. Newslet. Stratigr. 20, 43–58.

Yetiş, C., Kelling, G., Gökçen, S.L., Baroz, F., 1995. A revised stratigraphic framework for Late Cenozoic sequences in the northeastern Mediterranean region. Geol. Rundsch. 84, 794–812.

Yilmaz, C., Ozer, E., 1994. Temperate skeletal carbonate deposits in the Northeasternmost part of the Taurus Belt during Miocene (Turkey). Géol. Méditerr. XXI (1–2), 147–155.